Atmos. Chem. Phys. Discuss., https://doi.org/10.5194/acp-2018-1152
Manuscript under review for journal Atmos. Chem. Phys.
Discussion started: 4 January 2019

Atmospheric Chemistry and Physics Discussions

2015 and 2016 winter-time air pollution in China: SO_2 emission changes derived from a WRF/Chem-EnKF coupled data assimilation system

Dan Chen[1*], Zhiquan Liu[2*], Junmei Ban[2], Min Chen[1].

[1]Institute of Urban Meteorology, China Meteorological Administration, Beijing, 100089, China
[2]National Center for Atmospheric Research, Boulder, CO, 80301, USA

Under Review For Atmos. Chem. Phys.

* *Corresponding author: Dr. Zhiquan Liu (liuz@ucar.edu) and Dr. Dan Chen (dchen@ium.cn)*

Atmos. Chem. Phys. Discuss., https://doi.org/10.5194/acp-2018-1152
Manuscript under review for journal Atmos. Chem. Phys.
Discussion started: 4 January 2019

Atmospheric Chemistry and Physics Discussions

Abstract

Ambient pollutants in China changes significantly in recent years due to strict control strategies implemented by the government. The control strategies also bring uncertainties to both the "bottom-up" emission inventory and the model-ready gridded emission inputs especially in winter season. In this study, we updated the WRF/Chem-EnKF Data Assimilation system to quantitatively estimate the gridded hourly SO_2 emissions using hourly surface observations as constraints. Different from our previous study, in which meteorology and emission were both perturbed to obtain larger spread aiming to improve forecast skills; in this study, only emission was perturbed to ensure analyzed emission purely reflect necessary adjustments due to the emission uncertainties. In addition, direct emissions instead of emission scaling factors were used as analysis variable, which allowed for the detection of new emission sources. 2010 MEIC emission inventory (for January) was used as priori to generate 2015 and 2016 January analyzed emissions. The SO_2 emission changing trends for northern, western and southern China from 2010 to 2015 and that from 2015 to 2016 (for the month of January) were investigated. The January 2010-2015 differences showed inhomogeneous change patterns in different regions: 1) significant emission reduction in southern China, 2) significant emission reduction in larger cities but widely increase in surrounding suburban and rural regions for northern China which may indicate the missing raw coal combustion for winter heating that not taken into account in the priori emission inventory; 3) significantly large emission increase in western China due to the energy expansion strategy. This not only reflected the changes during the five years, but also combined the uncertainties in the priori emissions. The January 2015-2016 differences showed widely emission reduction from 2015 to 2016, indicating the stricter control strategy fully executed nationwide. These changes were corresponded to facts in reality, indicating that the updated DA system was capable to detect the emission deficiencies and optimize the emission. By generating the hourly analyzed emissions, the diurnal pattern of emissions (in terms of hourly factors) were also obtained. Forecast experiments showed the improvements by

using analyzed emissions were much larger in southern China than that in northern and western China. For Sichuan Basin, Central China, Yangzi River Delta, and Pearl River Delta, BIAS and RMSE decreased by 61.8%-78.2% and 27.9%-52.2%, respectively, and correlation coefficients increased by 12.5%-47.1%. However, the improvement in northern and western China were limited due to small spread. Another limitation of the study is that the analyzed emissions are still model dependent, as the ensembles are conducted through WRF/Chem model and thus the performances of ensembles are model dependent.

1. Introduction

Sulfur dioxide (SO_2) is a reactive, short-lived atmospheric trace gas and the life time is a few hours in summer to a few days in winter (e.g. Lee *et al.*, 2011). A few studies using satellite data revealed SO_2 pollutants and emissions in China changed dramatically in the past decades (e.g. Fioletov *et al.*, 2015, 2016; Ialongo *et al.*, 2015, Krotkov *et al.*, 2016, Koukouli *et al.* 2016, Lee *et al.*, 2011, Li *et al.*, 2010, Lin *et al.*, 2017, McLinden *et al.*, 2015, 2016; Wang *et al.*, 2015; van der A, *et al.*, 2017). Those studies revealed the widespread decline of annual SO_2 in densely populated and industrialized eastern China from 2005-2015, but some studies also noticed that Ozone Monitoring Instrument (OMI)-measured SO_2 in northwestern China appeared not to show a decreasing tread. The enhanced SO_2 vertical column densities are potentially attributable to increasing SO_2 emissions due to the development of large-scale energy industry bases in energy-abundant northwestern China under the national strategy for the energy safety in the 21st century. Those studies impressed the need to not only focus SO_2 load studies on the national level, but also focus on emerging economies within the Chinese realm of introducing new industrial and power plant parks.

Emission inventory is of fundamental importance for the scientific analysis of complex air pollution, especially for modeling studies. Traditionally the total amount of sectoral emissions have generally been estimated based on “bottom-up” approach that relied on available statistical information of activities (energy,

industrial production, vehicles etc.) and emission factors. For regional model application, the annual/monthly total amounts at national or provincial level are allocated spatially and temporally to generate hourly gridded emissions. Thus the uncertainties of the statistical information and the spatial-temporal allocation could both cause inaccurate representation of the hourly gridded emission input, and affect the performance of the model application. For example, Zhi *et al.* (2017) conducted village energy survey and revealed a huge amount of missing rural raw coal for winter heating in northern China, which implies an extreme underestimation of rural household coal consumptions by the China Energy Statistical Yearbooks. Although these surveys were conducted for the rural areas of only two cities, Baoding and Beijing, it revealed that rural emissions from raw coal in winter were higher than those from industrial and urban household sectors in the two cities in 2013. For the aspect of temporal allocation, as many emission sources have a large diurnal, weekly variability that is not fully represented; arbitrary hourly/weekly factors were used in the models. Furthermore, the control strategies in recent years in China bring dramatic changes in the SO_2 emission spatial-temporal pattern (factories mitigated from urban to rural region, industry staggering peak production etc.), thus large uncertainties are expected when applying those time-lagged "bottom-up" emission inventories (e.g. 2010-MEIC) in modelling studies for recent years (e.g. 2013 and afterward).

Among various Data Assimilation (DA) approaches to estimate or improve source emissions (e.g. Evensen, 1994; Houtekamer *et al.*, 2005, Hunt *et al.*, 2007; Pagowski and Grell, 2012, Miyakazi, *et al.*, 2012, 2013, 2014, Dai *et al.*, 2014), the Ensemble Kalman Filter (EnKF) is one of the most popular DA algorithms used to improve estimates of aerosols and gas-phase emissions (e.g. Tang *et al.*, 2013, 2016). In our previous study, Peng *et al.* (2017) extended the ensemble square root filter algorithm to simultaneously optimize the chemical initial conditions and emission input aiming to improve the forecasting of atmospheric $PM_{2.5}$. In the model, the deficiencies of concentration simulation come from varies aspects, including initial condition, emission, meteorology, chemistry and transport etc. In Peng *et al.* (2017), both meteorology and emission

were perturbed to reflect their uncertainties and also obtain larger spread. After DA, the differences between model and observations were attributed to the adjustments of emission and initial conditions. In this approach, the analyzed emission may be not purely reflect necessary adjustments due to the emission uncertainties but also the part from meteorology, as the meteorology perturbations changed the ensemble forecast thus also got involved in the error covariance calculation. In this study, we update the similar DA system to estimate SO_2 emissions. As our purpose is to investigate emission changes rather than to improve the forecast skills, thus we only perturb emissions. For our study, the foremost is to verify if the EnKF algorithm can be capable to detect the emission deficiencies and optimize the emission. In addition, Peng *et al.* (2017) analyzed emission scaling factors and thus does not allow the analysis of newly emerged emissions. To better detect the new emission sources, we update the system to directly analyze SO_2 emissions instead of emission scaling factors.

In this study, we focus on the winter-time SO_2 pollution and emission changes from 2010 to 2015/2016, aiming to quantitatively analyze the SO_2 emission trends by using the WRF/Chem-EnKF DA system, especially the inhomogeneous changing trends for northern, western and southern China. In this study, 2010 January emission inventory (Zhang *et al.*, 2009; Lei *et al.*, 2011; He 2012; Li *et al.*, 2014) is used as the prior for estimating 2015 and 2016 January emissions by assimilating hourly surface SO_2 concentration observations. Then the 2010-2015 and 2015-2016 emission changes are investigated by comparing two groups (2015 analyzed emissions v.s. 2010 prior emissions; 2016 analyzed emissions v.s. 2015 analyzed emissions) respectively. While the comparison in the first group not only reflects the real emission trends from 2010 to 2015, but also reflects the uncertainties in the original 2010 prior emission inventory. The second group more reflects the annual change from 2015 to 2016 as the uncertainties in the prior emissions are subtracted.

The paper is organized as follows. In section 2, the DA system, prior emissions, observational data and experimental design are described. The trends in SO_2 ambient concentrations by using the GSI 3DVAR DA system are analyzed in section 3, focusing on the ambient concentration spatial distribution and year-to-year

(2015-2016) changes. Section 4 described the results from the emission assimilation experiment using the updated WRF/Chem-EnKF system. This section starts from the evaluation of the ensemble performance to verify the DA system capability. Then the emission trends are given spatially in the whole domain and also in 8 different regions illustrating the inhomogeneous changes spatially. The hourly emission factors from the assimilation experiment are also given in section 4. Although it is difficult to verify the accuracy of the 2015 and 2016 analyzed emissions, we conducted two sets of forecast experiments with the priori emissions and the analyzed emissions respectively, and tried to analyze the differences attempting to check if any improvements were obtained with the analyzed emissions. The details are given in section 5 and conclusions are followed in section 6.

2. Model description, observations and methodology

We investigated the SO_2 pollution by two different DA techniques. In the first approach, we extended the Gridpoint Statistical Interpolation (GSI) 3DVAR DA system, that originally developed by Liu *et al.* (2011) and recently updated by Chen *et al.* (2018), to assimilate the SO_2 observations aiming to generate the SO_2 reanalysis fields; by analyzing the differences between control case (with priori emissions) and the reanalysis data, the deficiencies in the priori SO_2 emission and the emission changing trends can be derived. In the later approach, we updated the EnKF DA system (that used in Peng *et al.,* 2017) to estimate the WRF/Chem-based analyzed (posterior) SO_2 emissions using surface observations as constraints. The WRF/Chem configurations are the same as in Chen *et al.* (2018) thus the details are neglected here. The update of the GSI 3DVAR DA system is also built upon Chen *et al.* (2018), and only a simple description is given in this section. More descriptions about the WRF/Chem-EnKF DA system, and also priori emissions, observations and experimental design are introduced in detail.

Atmos. Chem. Phys. Discuss., https://doi.org/10.5194/acp-2018-1152
Manuscript under review for journal Atmos. Chem. Phys.
Discussion started: 4 January 2019

2.1 GSI 3DVAR DA system

Built upon the GSI 3DVAR DA system that used in Chen *et al.* (2018), we extended the system capability to assimilate surface SO_2 observations. The algorithm and the methodology for aerosol DA are described in Chen *et al.* (2018). Here only the differences for SO_2 DA are addressed.

The SO_2 observation operator is rather simple, $\prod m = \rho_c M_{SO_2}$. The unit of model simulated M_{SO_2} is ppm, thus multiplication by unit conversion ρ_c was required to convert the unit to $\mu g\ m^{-3}$ for consistency with the observations. The observation errors are calculated similarly as in Chen *et al.* (2018). In data quality control process, the SO_2 observational values larger than 650, or observations leading to innovations/deviations (observations minus the model-simulated observations determined form the first guess fields) exceeding 100 $\mu g\ m^{-3}$ were not used. The static BECs were computed via the "National Meteorological Center (NMC)" method (Parrish and Derber, 1992) by taking the differences of the 24-hr and 12-hr WRF/Chem forecasts valid at the same time for 60 pairs valid at either 00UTC or 12UTC over January 2015. The standard deviations in the whole domain is shown in supplemental Fig. S1.

2.2 WRF/Chem-EnKF DA system

The WRF/Chem-EnKF assimilation system framework (Fig. 1) is very similar to that of Peng *et al.* (2017). Peng *et al.* (2017) focused on the joint analysis of both initial conditions and emissions of $PM_{2.5}$, and addressed the forecasting skill improvement by using the EnKF system. Here we focus on the estimation of SO_2 emissions aiming to investigate the system capability to reflect the spatial-temporal emission changes by using observational data as constraints. In addition, instead of analyzing emission scaling factors as proxies, we attempt to directly analyze emissions which would allow the detection of new emission source. As in the previous approach, the emission scaling factors would be extremely large when a new emission source (e.g. a new power plant) occur in a originally "clean" model grid (priori emissions close to zero); the scaling factor is so large that it might be treated as "unrealistic" thus been filtered out in the system. The direct analysis of

emission is expected to be more appropriate for this case.

The Ensemble Square Root Filter (EnSRF, Whitaker and Hamill 2002) algorithm is very similar as in Peng *et al.* (2017) except for some differences, such as the state variables (changed from aerosols to SO_2 concentrations and emissions) and the inflation factor. In addition, the forecast model for emissions is also different from Peng *et al.* (2017). More details of the differences from Peng *et al.* (2017) are described below.

2.2.1 State variables

The similar Ensemble Square Root Filter is used in this study to update a 50-member ensemble as in Peng *et al.* (2017). We also applied the state augmentation method (e.g. Aksoy *et al.*, 2006; Miyazaki *et al.*, 2012). The only difference is that model parameter (SO_2 emissions) is directly estimated by including it as part of the state vector together with the model forecast variable (SO_2 concentration). The background ensemble is defined as below:

$$\mathrm{x}_i^b = \begin{bmatrix} \mathrm{C}_i^b \\ \mathrm{E}_i^b \end{bmatrix} \quad (1)$$

In which, x_i^b is the i^{th} member's background vector, consisted of model simulated SO_2 concentrations C_i^b and also the SO_2 emission E_i^b.

In Miyazaki *et al.* (2012), the state augmentation method was used to estimate NO_x emissions by using satellite observations (Ozone Monitoring Instrument-OMI retrieved NO_2 column) as constraints with a Local Ensemble Transform Kalman Filter (LETKF). The employment of combining state vectors (both NO_2 concentrations and NO_x emissions) allowed indirect relationships between NO_2 concentrations and NO_x emissions caused complex chemical and transport processes to be considered through the use of the background error covariance, which are produced by ensemble Chemical Transport Model-CTM forecast. Built upon Miyazaki *et al.* (2012), we used the similar approach aiming to address the indirect relationships between SO_2 concentrations and SO_2 emissions caused chemical (e.g. the conversion of SO_2 to aerosol species

Atmos. Chem. Phys. Discuss., https://doi.org/10.5194/acp-2018-1152
Manuscript under review for journal Atmos. Chem. Phys.
Discussion started: 4 January 2019

sulfate) and transport processes.

To reduce spurious correlations due to sampling error, covariance localization was applied following Schwartz *et al.* (2013, 2014) and Peng *et al.* (2017): EnSRF analysis increments were forced to zero 1280km from an observation in the horizontal and 1 scale height (in log pressure coordinates) in the vertical using a Gaspari and Cohn (1999) polynomial piecewise function.

2.2.2 Inflation factor in EnSRF

Further, multiplicative inflation was applied to posterior (after assimilation) perturbations about ensemble mean analyses, following Whitaker and Hamill (2012)'s "relaxing-to-prior spread" approach with an inflation parameter α.

$$\delta \mathrm{x}_a^i \leftarrow \delta \mathrm{x}_a^i \left(\alpha \frac{\sigma_b - \sigma_a}{\sigma_a} + 1\right), \tag{2}$$

In which, $\delta \mathrm{x}_a^i$ is the i^{th} member's analysis perturbation about the mean analysis, α is the inflation factor, and σ_b and σ_a are the prior (before assimilation) and posterior standard deviations at each model grid point, respectively. Using the definition of standard deviation, Eq.(2) can be expressed as

$$\sigma_a \leftarrow \alpha\sigma_b + (1-\alpha)\sigma_a, \tag{3}$$

Assimilating observations reduces ensemble spread, thus without inflation, $\sigma_a < \sigma_b$. From Eq.(3), if $\alpha > 1$, the inflated posterior spread is forced to be larger than the prior spread (σ_b). Conversely, for $\alpha < 1$, the inflated posterior spread must be less than σ_b. As no prior or additive inflation was employed, $\alpha > 1$ was necessary to maintain ensemble spread and we used inflation factor of $\alpha = 1.12$.

2.2.3 Forecast models for emissions

The forecast model is important as it propagates observation information, inflates the analysis spread and determines the quality of the first guess. In Peng *et al.* (2017), a smoothing operator served as the forecast

model for the emission scaling factors. In this study, the direct emissions instead of scaling factors were treated as part of the state variables; thus similar method of the forecasting approach was used as in Miyazaki *et al.* (2012): a linearized forecast model (M) provides a first guess of the state vector for data assimilation based on the background error covariance from the previous analysis time t_n to the new analysis time t_{n+1},

$$\mathrm{P}^{b}_{(t_{n+1})} = 0.75 \times \mathrm{MP}^{a}_{(t_n)}\mathrm{M}^{T} + 0.25 \times \mathrm{P}^{b}_{(t_0)}, \quad (4)$$

in which a persistent forecast model (M=I) is used for SO_2 emissions and the estimated emissions are used in the next step ensemble forecasting. To prevent the parameter covariance magnitude reduction, we added the initial priori ensemble as random noises. The forecast model for direct emissions is weighted 75% toward the results from the previous analyses time and 25% toward the static initial prior ensemble. The initial prior ensemble of SO_2 emissions for the first EnSRF analysis was constructed from the priori emissions by taking Gaussian random draws from a standard Gaussian distribution and varied for each ensemble member as in Peng *et al.* (2017). This approach incorporates the useful information from the previous time step and also the prior emissions, which propagate the observation information from one step to the next while still keeping some of the characteristics of the prior features.

2.3 Priori emissions

The Multi-resolution Emission Inventory for China (MEIC) (Zhang *et al.*, 2009; Lei *et al.*, 2011; He 2012; Li *et al.*, 2014) for January 2010 is used as the prior emission input. The pre-process to covert the original emission inventory (in 0.25 × 0.25 degree) to match the model grid spacing (40-km) is the same as in Chen *et al.* (2018). The spatial distribution of prior SO_2 emission in the simulation domain is shown in Fig. 2. A number of studies have revealed the uncertainties of the "bottom-up" emission inventories, including the energy statistics from national/provincial levels (e.g. Hong *et al.*, 2017), emission factors from different industry sectors (e.g. Zhao *et al.*, 2017). While our purpose is to investigate not only the uncertainty of the prior MEIC emission, but also the capability of DA system to dynamically update the SO_2 emissions by using surface

observations as constraints. For this purpose, the changing trends of SO_2 emissions from the priori emission year (2010) to our focusing years (2015 and 2016) are emphasized.

Actually, there are several different driving factors in different regions that may lead to inhomogeneous changing trends during those years (especially from 2010 to 2015). As the Chinese government has implemented desulphurization legislation (since 2005-2006 but with stricter control of actual use of the installations since 208-2009) and strict control strategies to insure the air quality during winter seasons since 2013, significant SO_2 emission reductions are expected since 2010. However, there are converse results for certain regions: village energy survey reveals missing rural raw coal in northern China (Zhi *et al.*, 2017), OMI-measured increasing SO_2 emissions due to energy industry expansion in northwestern China , especially new power plants installation in Xinjiang and Shaanxi, e.g. Shen *et al.* (2016). Eight different regions are illustrated to address the issue. Northern China is divided into two regions, North China Plain (NCP) and Northeastern China (NEC), as North China Plain is more emission intensive and may experience more strict control strategies than Northeastern China in winter haze periods. Northwestern China is also divided into two regions, including EGT (Energy Golden Triangle) and XJ (Xinjiang). Southern China is divided into four regions according to their geographic characteristics, including SB (Sichuan Basin), CC (Central China), YRD (Yangzi River Delta), and PRD (Pearl River Delta). The spatial distribution of the SO_2 emissions in the 8 regions are also illustrated in Fig. 2.

To improve the simulation, we also applied predefined functions for the diurnal variations of the priori SO_2 emissions, but the hourly factors are the same for all the sectors and all the grids, which are not optimal. As the diurnal variability is not publically released and highly uncertain, it brings large uncertainty in the simulations. We also want to investigate the capability of the DA system if it can improve the diurnal variations of SO_2 emissions by using hourly surface SO_2 concentrations as constraints.

Atmos. Chem. Phys. Discuss., https://doi.org/10.5194/acp-2018-1152
Manuscript under review for journal Atmos. Chem. Phys.
Discussion started: 4 January 2019

2.4 Observations

Hourly surface SO_2 concentrations for January 2015 and 2016 were obtained from the China National Environmental Monitoring Center (CNEMC). There are around 1600+ sites in our modeling domain (black dots in Fig. 2). As the 1600+ monitoring sites fall into 531 model grids, the observations within the same grid are averaged (the latitude and longitude too) for the purpose of statistics and verification. The observation sites spanned mostly in the northern, central and eastern China and are relatively sparse in western China. To ensure data quality before DA, SO_2 observational values larger than 650 $\mu g\, m^{-3}$ were deemed unrealistic and not assimilated in neither the GSI 3DVAR nor EnKF DA system.

2.5 Experimental design

To analyze SO_2 changing trend and also qualitatively evaluate the deficiencies of the priori SO_2 emission, the CONC_DA experiment with continuously cycling GSI 3DVAR was performed to generate the SO_2 reanalysis fields, and a control experiment (NO_DA) was also performed for comparison. The simulated periods are January of 2015 and 2016. In the NO_DA experiment, it initialized a new WRF/Chem forecast every 6-hr starting 00UTC, 20 December of previous year to spin up chemistry fields and run through 23UTC, 31 January. The chemistry fields were simply carried over from cycle to cycle while the meteorological Initial Condition (IC) and Boundary Condition (BC) were updated from GFS analysis data every 6-hr to prevent meteorology simulation drifting. For CONC_DA, GSI 3DVAR updated the SO_2 concentration every hour starting from 00UTC, 1 January. The background of the first cycle at 00UTC, 1 January was from the NO_DA experiment and the later ones were from the previous cycle's 1-hr forecast. The GFS analysis data in 6-hr frequency were interpolated in 1-hr and were used to update meteorological IC/BC in each 1-hr GSI 3DVAR cycle.

To estimate the SO_2 emissions using surface observations as constraints, the EMIS_DA experiment with continuously cycling WRF/Chem-EnKF was performed for January of 2015 and 2016. The initialization and

spin-up procedures of the 50 member ensemble were conducted by a three-day ensemble forecasts starting from 00UTC, 29 December of pervious year to 00UTC, 1 January of the next year, using the same method as in Peng *et al.* (2017), that lateral boundary conditions, initial condition of meteorology and emissions are perturbed. Then a 50-memble ensemble SO_2 forecasts valid at 00UTC, 1 January were generated, which were used as part of the background (C_i^b in Eq. 1) in the first EMIS_DA cycle. The other part of the background (E_i^b in Eq. 1) are the perturbed emissions of the last time step (at 23UTC, 31 December). Following the procedure in Figure 1, the EMIS_DA experiment started to conduct EnSRF analysis and generated both the updated SO_2 concentration fields and also the updated analyzed SO_2 emissions for the previous time step. In the next 1-hr forecast step, the updated SO_2 concentration fields of each member were used as the IC of the WRF-Chem 1-hr forecast; the forecast model (Eq. 4) generated the forecast emissions of each member by combining the previous time step's analyzed emissions and also the perturbed priori emissions. In this hourly cycling approach, the 1-hour WRF/Chem-EnKF cycling was conducted for January of 2015 and 2016, hourly analyzed SO_2 emissions were then generated.

To assess the analyzed emissions by the EnKF DA system, two forecast experiments (NO_DA_forecast and EMIS_DA_forecast) were conducted for the same period. 24-hour forecasts were performed at 00UTC of each day from 1-31 January for 2015 and 2016. The original prior emission and the updated analyzed emission were used respectively in NO_DA_forecast and EMIS_DA_forecast experiments. The chemistry initial conditions for each forecast in the two forecast experiments were from the 1-hour cycling GSI 3DVAR DA experiment. The meteorological IC and BC are all from GFS analysis and forecast data. The concentration differences between the two sets of 24-hour forecasts reflects the effects of updated emissions.

3. Trends in ambient concentrations

This section presents the simulated SO_2 concentration results by NO_DA and CONC_DA. As shown in Chen *et al.* (2018), the 1-hr cycling GSI 3DVAR DA system produces reliable $PM_{2.5}$ reanalysis fields; as the

methodology and the procedure are the same for SO_2, we can expect that the improvement of SO_2 assimilation is as good as that of $PM_{2.5}$, evidenced by the basic statistics including mean bias (MEAN/BIAS), standard deviation (STDV), and root-mean-square errors (RMSE) between NO_DA/CONC_DA and observations shown in Supplemental Fig. S2. Therefore, the purpose of this section is not to verify the performance of the GSI 3DVAR assimilation experiment, but to investigate the differences between NO_DA and CONC_DA. As NO_DA is the simulation with 2010 emission inventory while CONC_DA can serve as gridded reanalysis data from real observations, the difference of the two runs actually reflect the possible deficiencies in the model. As the meteorology are from the 6-hr GFS reanalysis data, we assume that most of the deficiencies come from using the 2010 priori emissions for the year 2015 and 2016 in the model and the comparisons also provide an idea of the changing trends of the emissions.

3.1 Spatial distribution

Figure 3 show the observed and modeled monthly average of surface SO_2 for January in 2015 and 2016. The observations show great differences between northern and southern China reflecting the dominating role of heating relevant emissions in northern China during winter season. The high values in northern China also show localized characteristics (no smooth transitions from high value region to surroundings) that reveal the localization of SO_2 emission and transport. NO_DA experiment significantly overestimates surface SO_2 in Sichuan Basin and Central China but underestimates it at several locations in northern China and Xinjiang. After GSI 3DVAR hourly cycling DA, CONC_DA experiment is very close to observations that it corrected most of the biases in NO_DA except for the very high values at some of the "hot spots" in northern China. The failure at those spots may come from the data filtering process that rejects SO_2 data with either the observed values larger than 650, or innovations exceeding 100 μg m^{-3}. The differences between CONC_DA and NO_DA more clearly revealed the inhomogeneous emission changes in different regions: for 2015, great SO_2 decrease from NO_DA to CONC_DA in most of eastern and southern regions but increase in Northeastern

China, Energy Golden Triangle and Xinjiang, indicating that 2010 January priori emissions should be adjusted accordingly (in decreasing/increasing trends respectively) to reflect the 2015 January status. The negative discrepancies in the eastern and southern regions are even larger for 2016, indicating continuous emission decreasing there.

To further investigate the deficiencies in priori emissions, the spatial distribution of the statistics (MEAN BIAS, RMSE and CORR) at each observational sites (with more than 2/3 valid data in the month) in January of 2015 and 2016 for the two experiments are shown in Fig. 4. We start from the 2015 statistics and then address the differences in 2016. In NO_DA, consistent with Fig. 3, surface SO_2 in southern China (Sichuan Basin, Central China, Pearl River Delta and Yangzi River Delta) is generally overestimated by 20-50 μg m^{-3}, but it is underestimated in Northeastern China and Energy Golden Triangle. The BIAS also showed the localized characteristics with positive biases in mega-cities (e.g. Beijing) while negative biases surroundings indicating overestimated/underestimated emissions respectively. There are also high RMSEs in Northeastern China, Northern China Plain and Energy Golden Triangle indicating wide spread of the differences between observational data and NO_DA simulations, which may also indicate the model deficiency in reproducing the strong temporal fluctuations (with the same daily emission and fixed hourly factors in the priori emissions). The poor correlations (less than 0.5) at the most of the sites also indicate the assumption. From year to year, the biases in 2016 are even more prominent. With GSI 3DVAR hourly cycling, the BIAS, RMSE and CORR are greatly improved as expected while the improvements in northern China are smaller than that in southern China.

3.2 Changes from 2015 to 2016

The differences in January of the two years (2015-2016) are shown in Fig. 5. Observations (Fig. 5a) show mostly decrease from 2015 to 2016 for most sites especially in Northern China Plain and southern China. In NO_DA experiment (same emission and different meteorology), some decreases are shown reflecting the

meteorology condition differences between the two years; but the observed significant decrease in Northern China Plain and southern China are not captured. CONC_DA (Fig. 5b) did reproduce the large decrease in Northern China Plain and southern China from 2015 to 2016. From the difference of Fig. 5b and 5c, it can be assumed that factors other than meteorology (e.g. emission control measures) did play important role in making the decreasing trend. CONC_DA failed to reproduce the large positive changes at 3 locations in Energy Golden Triangle region, as CONC_DA failed to reproduce the high SO_2 concentrations in both years due to data filtering processes.

4. Trends in emissions

Before the emission trends analysis, the ensemble performance was evaluated. To compare with prior emissions, the analyzed hourly emissions were averaged monthly. The analysis of total amount and spatial changes were conducted for the aforementioned 8 regions. We focus on the emission trends for two periods, 2010-2015 and 2015-2016. Besides, the hourly factors (diurnal cycle) of the optimized emissions were given to reflect the value of hourly DA.

4.1 Ensemble performance

In a well-calibrated system, when compared to the observations, the prior ensemble mean root-mean square error (RMSE) would equal the prior "total spread" defined as the square root of the sum of the observation error variance and ensemble variance of simulated observations (Houtekamer *et al.*, 2005). Time series of the hourly prior ensemble mean RMSE and total spread for surface SO_2 in the 8 regions are shown in Figure 6. The time series of two months (Jan. 2015 and Jan. 2016) are given separately. The magnitudes of the total spread and the RMSE are influenced by the diurnal cycle and the pollution events (driven by meteorology pattern and emissions). As expected, all the total spreads in the 8 regions are smaller than the RMSE for almost the whole periods except the first few days in 2015. As in spin-up procedure lateral boundary

and initial conditions of meteorology were also perturbed in addition to emission perturbation, that lead to larger spreads in the first DA cycle which may keep for a short period. For all the other periods without meteorology perturbation, insufficient spread of SO_2 ensemble forecasts were shown; while the cases in northern and western regions (North China Plain, Northeastern China, Energy Golden Triangle, Xinjiang) were worse than that in southern regions (Sichuan Basin, Central China, Yangzi River Delta, Pearl River Delta), as the priori ensemble mean RMSE in the northern regions were much larger but the total spreads were fairly constant. The distinction of the comparisons among different regions (North China Plain v.s. Yangzi River Delta/Pearl River Delta) indicated the deficiencies of perturbation procedure in the DA system when applying to the northern regions. Further investigations should be conducted to generate larger spreads for northern regions in the future studies.

4.2 Analyzed 2015 and 2016 emissions

The optimized SO_2 emissions obtained from the assimilation for Jan. of 2015 and 2016 are shown in Fig. 7. To address the changes from 2010 to 2015 and also that from 2015 to 2016, the differences and also ratios of the two groups (2010 v.s. 2015, 2015 v.s. 2016) are given. Actually for the comparison of 2015 analyzed emissions with 2010 priori emissions, as real observations are used to constrain the 2015 emission, the differences between the two sets of emissions actually reflects the necessary adjustments based on the 2010 priori emissions which are needed to better capture observations, thus it not only reflects the changing trends from 2010 to 2015, but also may indicate the deficiencies of the 2010 priori emission. It should be noted that the two aspects are just mixed in interpreting the results. While the comparison of 2015 analyzed with 2016 analyzed emissions are more straightforward, as they are both from observation constraints, the differences between the two reflect the annual changes between the two year and the impacts from prior emission deficiencies are just removed in the subtraction.

Compared to the 2010 priori emissions, the analyzed emissions for 2015 show different changes

spatially (northern, western, southern China). Large emission decreases in southern China (Sichuan Basin, Central China, Yangzi River Delta and Pearl River Delta) are shown but there are also some small amount of emission increases in scattered regions. Those increases are relatively small in absolute values (shown as light yellow color in Fig. 7c) but the 2015/2010 ratios can reach large numbers (shown as orange to red colors in Fig. 7d), as the priori emissions in those regions are very small (Fig. 2) thus small amount of changes lead to large ratios. For northern China (North China Plain, Northeastern China), the change pattern is somewhat opposite. Emission increases are shown for most of the regions with decreases only in scattered points. Large 2015/2010 increase ratios are also shown in western China (Xinjiang and Energy Golden Triangle) while the prior emissions are very sparse in those two region, thus the emission increases are more significant which may indicate new emission sources. For the changes from 2015 to 2016, the pattern is rather homogenous in the whole domain with almost decreases in all the regions.

4.3 Trends in different regions

To further illustrate the changes in different regions, the details of 8 regions are given in Fig. 8 (2015 v.s. 2010) and Fig. 9 (2016 v.s. 2015). Similar to Fig. 7, the emission changes in absolute values (left) and the ratios (right) are given for each region. To better understand the geographic changes, the center locations of some large cities (capital cities of provinces and municipal centers at city level) in those regions are labeled. According to Fig. 7, the change patterns are different in northern, western and southern China for 2015, thus the discussions are also given based on this classification. We start from the comparison of 2015 analyzed emissions with 2010 priori emissions, as the there are five year time lag between the two sets of emissions, large uncertainties and thus large changes are expected.

It is interesting to see that for northern China (North China Plain and Northeastern China), most significant decreases occur in or around the large cities (city center locations are labeled as black dots). The phenomenon is very prominent in North China Plain, as we can see some “cold” spots (grids with cold colors)

in Fig. 8a, they are either overlapped with the city center locations (Beijing, Tianjin, Xingtai, Handan in Beijing-Tianjin-Hebei Region, and Dongying, Jinan, Zibo, Jining in Shandong Province) or just adjacent of the center locations (Shijiazhuang, Linyi, Zaozhuang). As the center locations are represented as latitudes/longitudes that don't cover the whole city areas, thus there might be some shifting in interpretating the results when the city areas are too large (e.g. Shijiazhuang, Changchun, Shenyang) that been split into two or more grids in the model. While it still indicate that from 2010 to 2015, the emissions in those larger cities decreased due to the strict control strategies in those cities (factory migration from urban regions to remote regions, desulfurized equipment in factories/vehicle, low-sulfur energy etc.). However there are some emission increases in the suburban and rural regions surrounding those larger cities, either due to the emission migration from urban regions or the new emission sources newly added due to the urbanization development. It might also indicate that the control strategies are executed at different levels in urban (more strict) and suburban-rural regions during 2010 to 2015. In Northeastern China, significant "cold spots" also occur in the three larger cities, including Ha'erbing, Changchun, and Shenyang, but mostly increase in other areas indicating the similar trend as in North China Plain, that large emission decrease/mild emission increase in bigger cities/suburban-to-rural regions from 2010 to 2015 respectively. In addition to the possible reasons that aforementioned to account for the different changing trend of urban/suburban-rural regions from 2010 to 2015, it should be noted that the month of January is right the heating season for North China Plain and Northeastern China, the large areas of emission increase might also indicate some heating emissions (from the energy that has not been well statistically recorded, e.g. crop combustion, residential coal combustion) that are missing in the priori emissions.

In western China, where the emission intensities are not so high and the emission sources are relatively sparse, the emission changing trends from 2010 to 2015 are more obvious and are more meaningful to distinguish new emission sources/regions. As some studies revealed increasing SO_2 emissions due to energy

industry expansion and relocation in northwestern China from OMI measurements (Ling *et al.*, 2017), our 2015 analyzed emissions also show large emission increase in the whole areas of Energy Golden Triangle and Xinjiang except for very few larger cities (Yinchuan, Wuhai, Lanzhou; Kelamayi). The emissions in other areas of Energy Golden Triangle and Xinjiang are almost increasing from 2010 to 2015; especially for Xinjiang, the increase of emissions are all attributed to the rapid-developing cities, including Wulumuqi, A'kesu, Ku'erle, Yecheng, Manasi, Tacheng, Huocheng, Bachu, A'tushi, Shanshan, Shache etc. This is consistent with the satellite observations (Koukouli *et al.* 2016; Shen *et al.* 2016). These locations belong to provinces in Energy Golden Triangle and Xinjiang with emerging economies which are in haste to install power plants and are possibly viewed leniently by the authorities, in favor of growth.

In southern China, the decreasing trends are shown for large areas especially in Yangzi River Delta and Pearl River Delta, that decreasing trends in larger cities are clearly shown, e.g. Shanghai, Nanjing, Hangzhou in Yangzi River Delta and Guangzhou, Shenzhen and Foshan in Pearl River Delta with relatively larger decreasing ratios in more well-developed cities. In Sichuan Basin and Central China, the decrease in larger cities is also significant and different extent are achieved at different levels of cities. For Chengdu, Chongqing, Zunyi, Guiyang, Yunyang in Sichuan Basin and Wuhan and Changsha in Central China, around 40-50% reduction are shown from 2010 to 2015. For other larger cities (municipal centers of cities), 20-30% reduction is shown.

As aforementioned, the comparisons between the 2015 and 2016 analyzed emissions (Fig. 9) are more straightforward and reflect the necessary emission changes from 2015 to 2016 as the uncertainties in the priori emissions are subtracted. As expected, the decreasing trends are shown for almost all the labeled cities indicating the continuing control strategy strictly executed. However, there are still some grids with emission increases (around 10-30%) in surrounding regions especially in North China Plain which might reflect the emission increase from January 2015 to January 2016. As shown in Fig. 10 of Chen *et al.* (2018), the

temperature in January 2016 is much colder than that in 2015, the emission increase at those points may indicate heating relevant emissions. Compared with Fig. 8 (2015 v.s. 2010), the changes from 2015 to 2016 (either increase or decrease) in Fig. 9 are much milder.

The regional averages of 2015 and 2016 January emissions are summarized in Table 1. In northern China (North China Plain, Northeastern China) and western China (Energy Golden Triangle and Xinjiang), the 2015 analyzed emissions are all larger than 2010 prior emissions. The increase percentage are 12.7%, 49.4%, 25.6% and 72% for North China Plain, Northeastern China, Energy Golden Triangle and Xinjiang respectively, indicating the increase trend from 2010 January to 2015 January, either due to the emission increase in reality (possibly in Energy Golden Triangle and Xinjiang) or the uncertainties in the 2010 prior emissions (possibly in North China Plain and Northeastern China). The largest increase occurred in Xinjiang, reaching 72% consistent with the previous findings of the newly added emission sources in that region. In southern China, the 2015 analyzed emissions are all smaller, and the decreasing ratios are -10.5%, -9.9%, -13.8% and -22.9% for Sichuan Basin, Central China, Yangzi River Delta and Pearl River Delta respectively. For the changes from 2015 to 2016, decrease trend are shown for all the regions with the ratios range from -5.3% to -16.1%.

4.4 Hourly factors

As hourly observations were used to constrain the emissions, the analyzed emissions in hourly frequency are obtained which provided us an opportunity to investigate the emission hourly factors from observations. To retrieve the hourly factors, the emissions in each hour (24-hr) are averaged based on the EMIS_DA experiment for the whole period (Jan. 2-31). The retrieved hourly factors for 2015 and 2016 and also the 2010 prior emissions are shown in Fig. 10. The priori hourly factors are given arbitrary with two peaks during the day, 01UTC (09 Beijing-BJ time) and 09UTC (17 BJ time) to reflect the emissions during rush hours. While the retrieved hourly factors in northern and western China showed two peaks at around 02TC (10 BJ time)

and 12UTC (20 BJ time), but the second peaks are obscure in southern regions. In addition, the second peak of the hourly factors in northern and western regions are much lower than that of the first one, different from the predefined curve. In Xinjiang, the peaks come later than the other regions indicating the time zone differences caused the different energy consumption/emission pattern. It should be noted that the hourly factors are derived from the analyzed emissions constraining from ambient concentration observations, thus the response time from emission to ambient concentration are simplified in the assimilation system. Although the background emissions contain the information from the previous cycles and thus may help to pass the response information, there might still be some time-lag in the retrieved hourly factors which should be further verified.

5. Forecast improvements

As there are large uncertainties in the "bottom-up" 2010 priori emission inventory and also the assimilation process itself, it's difficult to verify the accuracy of the 2015 and 2016 January analyzed emissions. The "bottom-up" emission inventory for the two years are not yet available for comparison. Thus two sets of forecast experiment with the priori emissions and the analyzed emissions were conducted (NO_DA_forecast v.s. EMIS_DA_forecast, details in section 2.5). The forecast differences between the two experiments can reflect to some extent the performance/improvement of the analyzed emissions. To show the differences spatially, the statistics at single observational sites in the two forecast experiments are given and compared. In addition, the improvement from the hourly forecast is more meaningful to show the system capability of hourly emission optimization. Thus the time series of regional mean in 8 regions are also given to show the performance temporally.

5.1 Changes of spatial statistics

Figure 11 and 12 show the performances of the NO_DA_forecast and EMIS_DA_forecast experiments

for January of 2015 and 2016 respectively. Statistics, including BIAS, RMSE and CORR, are chosen to evaluate the two forecast experiments with prior emission and analyzed emissions respectively. As for single one site, the three statistics (BIAS, RMSE and CORR) may change in two directions (e.g. BIAS getting worse but RMSE and CORR getting better). To fairly evaluate and show the overall changes, the lumped 531 sites are classified into five different groups to reflect the differences of statistics. The classification and the performance are listed in Table 2. The spatial distribution of the NO_DA_forecast statistics for each sites are given in Fig. 11a and Fig. 12a. To better illustrate the changes of the statistics after applying analyzed emissions, the differences (EMIS_DA_forecast – NO_DA_forecast) instead of the absolute values are shown for the five defined groups in Fig. 11b-11f and Fig. 12b-12f. Specifically, the absolute values of BIAS are used in the difference calculation.

For single statistics, BIAS, RMSE and CORR are improved at 383, 444 and 426 sites respectively for the year 2015 (Table 2), while the total valid sites are 524 in the whole domain; that's to say that the ratio of sites being improved are 73%, 85% and 81% respectively using BIAS, RMSE and CORR as single criteria. When considering the overall performances using the three statistics, 300 sites (57%) are fully improved (BIAS/RMSE decrease and CORR increase), 138 sites (26%) are partially improved (either BIAS and RMSE improved, or RMSE and CORR improved), only 16 sites (3%) are overall worse and around 13% remaining sites can't be justified. The performance of 2016 is even better than 2015 that the sites fully improved/overall worse are more/less compared with the 2015 case.

Figure 11b show that the overall improvements are achieved in the whole domain, while the largest BIAS corrections occur at the sites in Sichuan Basin, Central China, Yangzi River Delta and Pearl River Delta (reaching 60-70% reduction), and the largest CORR improvement occurs in Xinjiang (reaching 0.35). The sites partially improved (Fig. 11c, d) and unclassified (Fig. 11e) are not in specific region but scattered in the whole domain. The sites overall getting worse (Fig. 11f) are very few and the variances are relatively small.

Consistent with Table 2, the performance of 2016 (Fig. 12) is even better than 2015 (Fig. 11), the bias corrections are more significant especially in Sichuan Basin, Central China, Yangzi River Delta and Pearl River Delta, and the CORR improvements are even larger in Xinjiang.

5.2 Time series of regional mean

Figure 13 show the time series of regional mean forecast (NO_DA_forecast and EMIS_DA_forecast) and observed SO_2 concentrations in 8 regions for 2015 and 2016. From the aspect of regional mean, forecast with prior emissions are severely overestimated in southern China (Sichuan Basin, Central China, Yangzi River Delta, Pearl River Delta) and the overestimations are largely corrected in the forecast with analyzed emissions. For Northeastern China, Energy Golden Triangle and Xinjiang, forecast with prior emissions are underestimated, and forecast with analyzed emissions helped to correct the biases. It is surprising to see that the regional averages in North China Plain matches well the observations although the site-to-site comparison (Fig.11 and 12) show large biases in single sites. As the sites in one region are averaged thus the positive/negative biases among different sites might offset in the averaged time series. For this reason, RMSE and CORR of all the hourly data in one region are also calculated as verification.

The statistics of BIAS, RMSE and CORR in the 8 regions are given in Table 3. From the aspect of regional mean, the improvements after applying the analyzed emissions are much significant in southern China than that in northern China, that RMSE decreased by 27.9-39.3% and BIAS decreased by 63.3% -78.2%, CORR increases by 16.7%-45.0% for the year 2015. For northern China, although the improvements are not so large, the BIAS still decreases (except North China Plain) and the decrease ratio ranges from 6.3% to 22.9%, RMSE decreases by 4.2-8.8% and CORR increases by 7.7% to 366.7%. The largest CORR increase occurs in Xinjiang from 0.06 to 0.28, indicating that the newly added emission sources in the analyzed emissions are necessary. Compared to 2015, the improvements in 2016 are also larger consistent with previous discussions.

Atmos. Chem. Phys. Discuss., https://doi.org/10.5194/acp-2018-1152
Manuscript under review for journal Atmos. Chem. Phys.
Discussion started: 4 January 2019

6. Conclusions

Based upon our previous study (Peng *et al.* 2017), we further updated the WRF/Chem-EnKF DA system to quantitatively estimate the gridded hourly SO2 emissions using hourly surface observations as constraints. Different from Peng *et al.* (2017), in which meteorology and emission were both perturbed to obtain larger spread aiming to improve forecast skills; in this study, only emission were perturbed to ensure analyzed emission purely reflect necessary adjustments due to the emission uncertainties. In addition, direct emissions instead of emission scaling factors were used as analysis variables which allows for the detection of new emission sources.

2010 January MEIC prior emissions were used to generate 2015 and 2016 January analyzed emissions by using hourly surface SO_2 observations as constraints. Compared with the 2010 priori emissions, the analyzed emissions in January 2015 showed inhomogeneous change patterns in different regions: 1) significant emission reduction in southern China, including Sichuan Basin, Central China, Yangzi River Delta and Pearl River Delta; however, there are still some grids with slight emission increase surrounding larger cities, indicating the emission transition due to urbanization development; the reduction ratio of the total January emissions for the aforementioned four regions are -10.5%, -9.9%, -13.8% and -22.9% respectively; 2) for northern China (Northern China Plain and Northeastern China), the situation is more complicated during the winter heating season; comparisons show large emission reduction in larger cities but widely increase in surrounding suburban and rural regions, which may indicate the missing raw coal combustion not taken into account in the priori emission inventory; the increase ratios of the total January emissions for Northern China Plain and Northeastern China are 12.7% and 49.4% respectively; 3) significantly large emission increase in western China (Energy Golden Triangle, Xinjiang) due to the energy expansion strategy, which are consistent with the satellite observations (e.g. Ling *et al.*, 2017); the increase ratio of the total January emissions for Energy Golden Triangle and Xinjiang are 25.6%, and 72.0% respectively. It should be noted that the

comparisons between 2010 prior emission and the 2015 analyzed emission not only reflect the changes during the five years, but also combine the uncertainties in the priori emissions (either due to the uncertainties in total annual/monthly emissions or the allocation process from the provincial emissions to the gridded data). Comparisons of the 2015 and 2016 analyzed emissions show widely emission reduction from 2015 to 2016, indicating the stricter control strategy fully executed nationwide. These changes were corresponded to facts in reality indicating that the updated DA system is capable to detect the emission deficiencies and optimize the emission with limited perturbations. The detection of the emission changes by the DA system can be localized to city levels as the benefit from the intensive observations and the model grid resolution. By generating the hourly-analyzed emissions, the diurnal variations of emissions were also obtained.

It is difficult to verify the accuracy of the analyzed emissions, as the top-down emission inventory for 2015 and 2016 are not yet available for comparison. Two sets of forecast experiment with the priori emissions and the analyzed emissions were conducted to show the differences and improvements. Among the lumped 531 sites, 300 sites are fully improved (BIAS and RMSE reduced, and CORR increased) and only 16 sites are entirely worse for the year 2015; other 138 sites are partially improved (two statistics get better). The improvements are much larger in southern China than that in northern and western China. By using the analyzed emissions, BIAS and RMSE are reduced by 61.8%-78.2% and 27.9%-52.2% respectively, and correlation coefficient increase by 12.5% -47.1% for southern China regions (Sichuan Basin, Central China, Yangzi River Delta, and Pearl River Delta). However, for northern and western China where the original BIAS and RMSE are larger, the decrease are relatively smaller. Nevertheless, the correlations are indeed improved especially for Xinjiang, as new emissions are captured in the analyzed emissions. The distinction of the comparisons among different regions (northern/western regions v.s. southern regions) indicated the deficiencies of perturbation procedure in the DA system when applying to the northern/western regions. Further investigations should be conducted to generate larger spreads for those regions in the future studies.

Our study serves as an example that the Ensemble Kalman Filter algorithm combing with WRF/Chem regional model can be used to optimize model-ready gridded hourly emission inputs, by using hourly surface observations as constraints. This approach is useful to assess the emission control strategy and can also improve the forecast skills. While the limitation of the study is that the analyzed emissions are still model dependent as the ensembles are conducted through WRF/Chem model and thus the performance of ensembles is model dependent. Changes in model configurations (e.g. spatial resolutions, chemistry options) can cause differences in the DA system. In our study, the model resolution is 40-km which might be too coarse for SO_2 as it's a relatively short-life-time specie and the localized characteristics might not be captured by the system. In addition, the reactions of SO_2 is only reflected in the WRF/Chem system but not in the EnKF process, considering the reaction time of SO_2 in the ambient, there might be some time lag of the hourly emission factors.

Author contributions

ZL and DC designed research; DC performed research; JB contributed towards development of DA system; MC provides funds; DC wrote the paper, with contributions from all co-authors.

Acknowledgement

This work was supported by the National Key R&D Program on Monitoring, Early Warning and Prevention of Major Natural Disasters under grant (2017YFC1501406), the National Natural Science Foundation of China (Grant No. 41807312) and Basic R&D special fund for central scientific research institutes (IUMKYSZHJ201701). NCAR is sponsored by US National Science Foundation. We would like to thank Zhen Peng for useful discussions and patient guide on DA system development.

References

BIEE (British Institute of Energy Economics): BP Statistical Review of World Energy June 2016, available at: http://www.bp.com/content/dam/bp/pdf/energy-economics/statistical-review-2016/bp-statistical-review-of-world-energy-2016-full-report.pdf (last access: 21 January 2017), 2016.

Chen, D., Liu, Z., Ban, J., Zhao, P., and Chen, M.: Retrospective analysis of 2015–2017 winter-time PM2.5 in China: response to emission regulations and the role of meteorology, Atmos. Chem. Phys. Discuss., https://doi.org/10.5194/acp-2018-890, in review, 2018.

Dai, T., Schutgens, N.A.J., Goto, D. Shi, G.Y., Nakajima, T.: Improvement of aerosol optical properties modeling over Eastern Asia with MODIS AOD assim- ilation in a global non-hydrostatic icosahedral aerosol transport model, Environ. Pollut., 195, 319–329, 2014.

Evensen, G.: Sequential data assimilation with a nonlinear quasi-geostrophic model using Monte Carlo methods to forecast error statistics, J. Geophys. Res., 99, 10143–10162, doi:10.1029/94JC00572, 1994.

Fioletov, V. E., McLinden, C. A., Krotkov, N., and Li, C.: Lifetimes and emissions of SO_2 from point sources estimated from OMI, Geophys. Res. Lett., 42, 1969–1976, https://doi.org/10.1002/2015GL063148, 2015.

Fioletov, V. E., McLinden, C. A., Krotkov, N., Li, C., Joiner, J., Theys, N., Carn, S., and Moran, M. D.: A global catalogue of large SO_2 sources and emissions derived from the Ozone Monitoring Instrument, Atmos. Chem. Phys., 16, 11497–11519, https://doi.org/10.5194/acp-16-11497-2016, 2016.

Gaspari, G., and S. E. Cohn.: Construction of correlation functions in two and three dimensions. Quart. J. Roy. Meteor. Soc., 125,723–757, https://doi.org/10.1002/qj.49712555417, 2006.

Koukouli, M. E., Balis, D. S., van der A, R. J., Theys, N., Hedelt, P., Richter, A., Krotkov, N., Li, C., and Taylor, M.: Anthropogenic sulphur dioxide load over China as observed from different satellite sensors, Atmos. Environ., 145, 45-59, 10.1016/j.atmosenv.2016.09.007, 2016.

Krotkov, N. A., McLinden, C. A., Li, C., Lamsal, L. N., Celarier, E. A., Marchenko, S. V., Swartz, W. H., Bucsela, E. J., Joiner, J., Duncan, B. N., Boersma, K. F., Veefkind, J. P., Levelt, P. F., Fioletov, V. E., Dickerson, R. R., He, H., Lu, Z. F., and Streets, D. G.: Aura OMI observations of regional SO_2 and NO2 pollution changes from 2005 to 2015, Atmos. Chem. Phys., 16, 4605-4629, 10.5194/acp-16-4605-2016, 2016.

He, K.B., Multi-resolution emission Inventory for China (MEIC): model framework and 1990-2010 anthropogenic emissions. In: Presented on the international Global Atmospheric Chemistry Conference, September 17-21, Beijing, China 2012

Hong, C. P., Zhang, Q., He, K. B., Guan, D. B., Li, M., Liu, F., and Zheng, B.: Variations of China's emission estimates: response to uncertainties in energy statistics, Atmos. Chem. Phys., 17, 1227-1239, 10.5194/acp-17-1227-2017, 2017.

Houtekamer, P. L., Mitchell, H. L., Pellerin, G., Buehner, M., Charron, M., Spacek, L., and Hansen, B.: Atmospheric data assimilation with an ensemble Kalman filter: Results with real observations, Mon. Weather Rev., 133, 604–620, 2005.

Huneeus, N., Boucher, O., and Chevallier, F.: Atmospheric inversion of SO_2 and primary aerosol emissions for the year 2010, Atmos. Chem. Phys., 13, 6555-6573, 10.5194/acp-13-6555-2013, 2013.

Hunt, B. R., Kostelich, E. J., and Szunyogh, I.: Efficient data assimilation for spatiotemporal chaos: A local ensemble transform Kalman filter, Physica D, 230, 112–126, 2007.

Ialongo, I., Hakkarainen, J., Kivi, R., Anttila, P., Krotkov, N. A., Yang, K., Li, C., Tukiainen, S., Hassinen, S., and Tamminen, J.: Comparison of operational satellite SO_2 products with ground-based observations in northern Finland during the Icelandic Holuhraun fissure eruption, Atmos. Meas. Tech., 8, 2279–2289, https://doi.org/10.5194/amt-8-2279-2015, 2015.

Lee, C., Martin, R. V., van Donkelaar, A., Lee, H., Dickerson, R. R., Hains, J. C., Krotkov, N., Richter, A., Vinnikov, K., and Schwab, J. J.: SO_2 emissions and lifetimes: Estimates from inverse modeling using in situ and global, space-based (SCIAMACHY and OMI) observations, J. Geophys. Res.-Atmos., 116, Artn D06304, 10.1029/2010jd014758,

2011.

Lei, Y., Zhang, Q., He, K. B., and Streets, D. G.: Primary anthropogenic aerosol emission trends for China, 1990-2005, Atmos. Chem. Phys., 11, 931-954, 10.5194/acp-11-931-2011, 2011.

Li, W. J., Zhou, S. Z., Wang, X. F., Xu, Z., Yuan, C., Yu, Y. C., Zhang, Q. Z., and Wang, W. X.: Integrated evaluation of aerosols from regional brown hazes over northern China in winter: Concentrations, sources, transformation, and mixing states, J. Geophys. Res.-Atmos., 116, Artn D09301, 10.1029/2010jd015099, 2011.

Li, C., Zhang, Q., Krotkov, N. A., Streets, D. G., He, K., Tsay, S. C., and Gleason, J. F.: Recent large reduction in sulfur dioxide emissions from Chinese power plants observed by the Ozone Monitoring Instrument, Geophys. Res. Lett., 37, L08807, https://doi.org/10.1029/2010GL042594, 2010.

Li, M., Zhang, Q., Streets, D. G., He, K. B., Cheng, Y. F., Emmons, L. K., Huo, H., Kang, S. C., Lu, Z., Shao, M., Su, H., Yu, X., and Zhang, Y.: Mapping Asian anthropogenic emissions of non-methane volatile organic compounds to multiple chemical mechanisms, Atmos. Chem. Phys., 14, 5617-5638, 10.5194/acp-14-5617-2014, 2014.

Ling, Z. L., Huang, T., Zhao, Y., Li, J. X., Zhang, X. D., Wang, J. X., Lian, L. L., Mao, X. X., Gao, H., and Ma, J. M.: OMI-measured increasing SO_2 emissions due to energy industry expansion and relocation in northwestern China, Atmos. Chem. Phys., 17, 9115-9131, 10.5194/acp-17-9115-2017, 2017.

McLinden, C. A., Fioletov, V., Krotkov, N. A., Li, C., Boersma, K.F., and Adams, C.: A decade of change in NO2 and SO_2 over the Canadian oil sands as seen from space, Environ. Sci. Technol., 50, 331–337, https://doi.org/10.1021/acs.est.5b04985, 2015.

McLinden, C. A., Fioletov, V., Shephard,M.W., Krotkov, N., Li, C., Martin, R. V., Moran, M. D., and Joiner, J.: Space-based detection of missing sulfur dioxide sources of global air pollution, Nat. Geosci., 9, 496–500, https://doi.org/10.1038/ngeo2724, 2016.

Miyazaki, K., Eskes, H. J., and Sudo, K.: Global NOx emission estimates derived from an assimilation of OMI tropospheric NO2 columns, Atmos. Chem. Phys., 12, 2263-2288, 10.5194/acp-12-2263-2012, 2012.

Miyazaki, K., and Eskes, H.: Constraints on surface NOx emissions by assimilating satellite observations of multiple species, Geophys. Res. Lett., 40, 4745-4750, 10.1002/grl.50894, 2013.

Ministry of Environmental Protect, 12th Five-year Plan of Prevention and Control of Atmospheric Pollution in Key Areas, Beijing, 2012.

Pagowski, M., and Grell, G. A.: Experiments with the assimilation of fine aerosols using an ensemble Kalman filter, J. Geophys. Res.-Atmos., 117, D21302, doi:10.1029/2012jd018333, 2012.

Peng, Z., Liu, Z. Q., Chen, D., and Ban, J. M.: Improving $PM_{2.5}$ forecast over China by the joint adjustment of initial conditions and source emissions with an ensemble Kalman filter, Atmos. Chem. Phys., 17, 4837-4855, 10.5194/acp-17-4837-2017, 2017.

Ronald, J. V., Mijling, B., Ding, J., Koukouli, M. E., Liu, F., Li, Q., Mao, H. Q., and Theys, N.: Cleaning up the air: effectiveness of air quality policy for SO_2 and NOx emissions in China, Atmos. Chem. Phys., 17, 1775-1789, 10.5194/acp-17-1775-2017, 2017.

Schwartz, C. S., Liu, Z. Q., Lin, H. C., and Cetola, J. D.: Assimilating aerosol observations with a "hybrid" variational-ensemble data assimilation system, J. Geophys. Res.-Atmos., 119, 4043-4069, 10.1002/2013jd020937, 2014.

Shen, Y. J., Zhang, X. D., Brook, J. R., Huang, T., Zhao, Y., Gao, H., and Ma, J. M.: Satellite Remote Sensing of Air Quality in the Energy Golden Triangle in Northwest China, Environ. Sci. Tech. Let., 3, 275-279, 10.1021/acs.estlett.6b00182, 2016.

Wang, S., Zhang, Q., Martin, R.V., Philip, S., Liu, F., Li, M., Jiang, X., and He, K.: Satellite measurements oversee China's sulfur dioxide emission reductions from coal-fired power plants, Environ. Res. Lett., 10, 114015, https://doi.org/10.1088/1748-9326/10/11/114015, 2015.

Wang, X. F., Wang, W. X., Yang, L. X., Gao, X. M., Nie, W., Yu, Y. C., Xu, P., Zhou, Y., and Wang, Z.: The secondary formation of inorganic aerosols in the droplet mode through heterogeneous aqueous reactions under haze conditions, Atmos. Environ., 63, 68-76, 10.1016/j.atmosenv.2012.09.029, 2012b.

Tang, X., Zhu, J., Wang, Z. F., and Gbaguidi, A.: Improvement of ozone forecast over Beijing based on ensemble

Kalman filter with simultaneous adjustment of initial conditions and emissions, Atmos. Chem. Phys., 11, 12901-12916, 10.5194/acp-11-12901-2011, 2011.

Tang, X., Zhu, J., Wang, Z. F., Wang, M., Gbaguidi, A., Li, J., Shao, M., Tang, G. Q., and Ji, D. S.: Inversion of CO emissions over Beijing and its surrounding areas with ensemble Kalman filter, Atmos. Environ., 81, 676-686, 10.1016/j.atmosenv.2013.08.051, 2013.

Tang, X., Zhu, J., Wang, Z. F., Gbaguidi, A., Lin, C. Y., Xin, J. Y., Song, T., and Hu, B.: Limitations of ozone data assimilation with adjustment of NOx emissions: mixed effects on NO2 forecasts over Beijing and surrounding areas, Atmos. Chem. Phys., 16, 6395-6405, 10.5194/acp-16-6395-2016, 2016.

The Central People's Government of the People Republic of China, Atmospheric Pollution Prevention and Control Action Plan, 2013.

Yang, Y. R., Liu, X. G., Qu, Y., An, J. L., Jiang, R., Zhang, Y. H., Sun, Y. L., Wu, Z. J., Zhang, F., Xu, W. Q., and Ma, Q. X.: Characteristics and formation mechanism of continuous hazes in China: a case study during the autumn of 2014 in the North China Plain, Atmos. Chem. Phys., 15, 8165-8178, 10.5194/acp-15-8165-2015, 2015.

Zhang, Q., Streets, D. G., Carmichael, G. R., He, K. B., Huo, H., Kannari, A., Klimont, Z., Park, I. S., Reddy, S., Fu, J. S., Chen, D., Duan, L., Lei, Y., Wang, L. T., and Yao, Z. L.: Asian emissions in 2006 for the NASA INTEX-B mission, Atmos. Chem. Phys., 9, 5131-5153, 2009.

Zhao, Y., Zhou, Y. D., Qiu, L. P., and Zhang, J.: Quantifying the uncertainties of China's emission inventory for industrial sources: From national to provincial and city scales, Atmos. Environ., 165, 207-221, 10.1016/j.atmosenv.2017.06.045, 2017.

Zhao, Y., Nielsen, C. P., Lei, Y., McElroy, M. B., and Hao, J.: Quantifying the uncertainties of a bottom-up emission inventory of anthropogenic atmospheric pollutants in China, Atmos. Chem. Phys., 11, 2295-2308, 10.5194/acp-11-2295-2011, 2011.

Zhi, G. R., Zhang, Y. Y., Sun, J. Z., Cheng, M. M., Dang, H. Y., Liu, S. J., Yang, J. C., Zhang, Y. Z., Xue, Z. G., Li, S. Y., and Meng, F.: Village energy survey reveals missing rural raw coal in northern China: Significance in science and policy, Environ. Pollut., 223, 705-712, 10.1016/j.envpol.2017.02.009, 2017.

Atmos. Chem. Phys. Discuss., https://doi.org/10.5194/acp-2018-1152
Manuscript under review for journal Atmos. Chem. Phys.
Discussion started: 4 January 2019

Atmospheric Chemistry and Physics Discussions

Tables and Figures

Table 1. Prior and analyzed January emissions, and changing ratios for 8 regions (unit: 10^6 kg per day)

Table 2. Overall statistics changes of the EMIS_DA_FCST experiment compared with NO_DA_FCST experiment

Table 3. Statistics of the EMIS_DA_FCST and NO_DA_FCST experiments in 8 regions (unit: μg m^{-3} for BIAS and RMSE)

Figure 1. Flow chart of the data assimilation system that simultaneously optimizes the chemical initial conditions and emissions.

Figure 2. Spatial distribution of prior SO_2 emissions used in this study. Regions defined in red rectangles are: a-NCP (North China Plain), b-NEC (Northeastern China), c-EGT (Energy Golden Triangle), d-XJ (Xinjiang), e-SB (Sichuan Basin), f-CC (Central China), g-YRD (Yangzi River Delta), h-PRD (Pearl River Delta). Unit: mol km^{-2} h^{-1}.

Figure 3. Observed and modeled monthly average of SO2 concentrations for January in 2015 (Left) and 2016 (right). (a) Observations, (b) NO_DA, (c) CONC_DA, (d) CONC_DA-NO_DA. Unit: μg m^{-3}.

Figure 4. The spatial distribution of statistics between model simulations and observations for (a) January 2015 and (b) January 2016. Top: NO_DA v.s. observation, bottom: CONC_DA v.s. observation. Units: μg m^{-3} for BIAS and RMSE.

Figure 5. Observed and modeled SO_2 ambient concentration changes (January 2016 - January 2015). (a) Observations, (b) NO_DA, (c) CONC_DA. (Unit: μg m^{-3})

Figure 6. Regional averaged RMSE and total spread for (a) January 2015 and (b) January 2016 in 8 regions (Unit: μg m^{-3})

Figure 7. Analyzed emissions for (a) January 2015 and (b) January 2016. (c) The differences of 2015-2010_prior, (d) Ratios of 2015/2010_priori, (e) The differences of 2016-2015 and (f) Ratios of 2016/2015. Unit is mol km^{-2} h^{-1} for (a), (b), (c) and (e).

Figure 8. The differences of analyzed 2015 January emissions and 2010 priori emissions in 8 regions. Left panels are emission differences of 2015-2010 (unit: mol km^{-2} h^{-1}) and right panels are ratios of 2015/2010 in each region.

Figure 9. Same as Figure 8, but for the differences of analyzed 2016 January emissions and 2015 January emissions in 8 regions. Left panels are emission differences of 2016-2015 (unit: mol km^{-2} h^{-1}) and right panels are ratios 2016/2015 in each region.

Figure 10. Hourly factors in priori emission inventory and those derived from EMIS_DA experiment in 8 regions.

Atmos. Chem. Phys. Discuss., https://doi.org/10.5194/acp-2018-1152
Manuscript under review for journal Atmos. Chem. Phys.
Discussion started: 4 January 2019

Atmospheric Chemistry and Physics Discussions

Figure 11. The spatial distribution of error statistics between model simulations and observations for January 2015. (a) Statistics between NO_DA_FCST and observations, BIAS and RMSE in μg m^{-3}; (b)-(f) are the statistics improvements from NO_DA_FCST to EMIS_DA_FCST for different groups of sites (classification in table 2), the BIAS and RMSE improvements are in percentage.

Figure 12. Same as Figure 11 but for January 2016.

Figure 13. Time series of regional mean SO_2 concentrations from observations and model simulations with priori and analyzed (posterior) emissions for (a) January 2015 and (b) January 2016 in 8 regions. (Unit: μg m^{-3})

Atmos. Chem. Phys. Discuss., https://doi.org/10.5194/acp-2018-1152
Manuscript under review for journal Atmos. Chem. Phys.
Discussion started: 4 January 2019

Atmospheric Chemistry and Physics Discussions

Table 1. Prior and analyzed January emissions, and changing ratios for 8 regions (unit: 10^6 kg per day)

	2010_prior	2015_posterior	2016_ posterior	(2015-2010) /2010	(2016-2015) /2015
NCP	16.23	18.29	17.33	12.7%	-5.3%
NEC	4.12	6.16	5.30	49.4%	-13.9%
ETR	11.01	13.82	13.01	25.6%	-5.9%
XJ	1.62	2.79	2.34	72.0%	-16.1%
SB	17.12	15.33	13.43	-10.5%	-12.4%
CC	9.95	8.96	7.57	-9.9%	-15.5%
YRD	5.80	5.00	4.65	-13.8%	-7.0%
PRD	1.82	1.40	1.23	-22.9%	-12.6%

Atmos. Chem. Phys. Discuss., https://doi.org/10.5194/acp-2018-1152
Manuscript under review for journal Atmos. Chem. Phys.
Discussion started: 4 January 2019

Atmospheric Chemistry and Physics Discussions

Table 2. Overall statistics changes of the EMIS_DA_FCST experiment compared with NO_DA_FCST experiment

Types	BIAS	RMSE	CORR		
2015					
Better	383	444	426		
Worse	141	80	97		
2016					
Better	375	444	456		
Worse	148	79	67		
Groups	BIAS	RMSE	CORR	2015	2016
A. Overall improved	decrease	decrease	increase	300	321
B. Partially improved (BIAS, RMSE)	decrease	decrease	decrease	61	43
C. Partially improved (RMSE, CORR)	increase	decrease	increase	77	71
D. Not justified				70	77
E. Overall worse	increase	increase	decrease	16	11

Atmos. Chem. Phys. Discuss., https://doi.org/10.5194/acp-2018-1152
Manuscript under review for journal Atmos. Chem. Phys.
Discussion started: 4 January 2019

Atmospheric Chemistry and Physics Discussions

Table 3. Statistics of the EMIS_DA_FCST and NO_DA_FCST experiments in 8 regions (unit: μg m^{-3} for BIAS and RMSE)

			BIAS			RMSE			CORR		
	N sites	N data	NO_DA	EMIS_DA	Changes (%)	NO_DA	EMIS_DA	Changes (%)	NO_DA	EMIS_DA	Changes (%)
2015											
NCP	67	46699	-9.6	-10.1	5.2%	53.7	49.0	-8.8%	0.52	0.62	19.2%
NEC	30	20910	-29.3	-22.6	-22.9%	61.8	57.1	-7.6%	0.52	0.56	7.7%
EGT	45	31365	-41.2	-38.6	-6.3%	84.8	81.2	-4.2%	0.53	0.58	9.4%
XJ	19	13243	-12.6	-10.3	-18.3%	36.8	33.7	-8.4%	0.06	0.28	366.7%
SB	48	33456	9.7	2.7	-72.2%	45.1	32.5	-27.9%	0.20	0.29	45.0%
CC	53	36941	6.1	-1.4	-77.0%	49.7	34.6	-30.4%	0.32	0.39	21.9%
YRD	34	23698	10.9	4.0	-63.3%	37.0	24.9	-32.7%	0.47	0.55	17.0%
PRD	20	13940	8.7	1.9	-78.2%	24.7	15.0	-39.3%	0.42	0.49	16.7%
2016											
NCP	67	46699	2.1	-0.3	-85.7%	41.5	36.2	-12.8%	0.58	0.69	19.0%
NEC	30	20910	-16.8	-14.7	-12.5%	41.2	36.9	-10.4%	0.50	0.58	16.0%
EGT	45	31365	-27.7	-26.6	-4.0%	64.5	61.2	-5.1%	0.56	0.63	12.5%
XJ	19	13243	-5.8	-6.0	3.4%	30.5	26.9	-11.8%	0.23	0.47	104.3%
SB	48	33456	14.5	5.2	-64.1%	38.9	23.1	-40.6%	0.17	0.25	47.1%
CC	53	36941	11.2	2.6	-76.8%	38.0	22.2	-41.6%	0.28	0.37	32.1%
YRD	34	23698	12.3	4.7	-61.8%	33.7	20.1	-40.4%	0.48	0.54	12.5%
PRD	20	13940	9.8	2.4	-75.5%	20.9	10.0	-52.2%	0.30	0.39	30.0%

Atmos. Chem. Phys. Discuss., https://doi.org/10.5194/acp-2018-1152
Manuscript under review for journal Atmos. Chem. Phys.
Discussion started: 4 January 2019

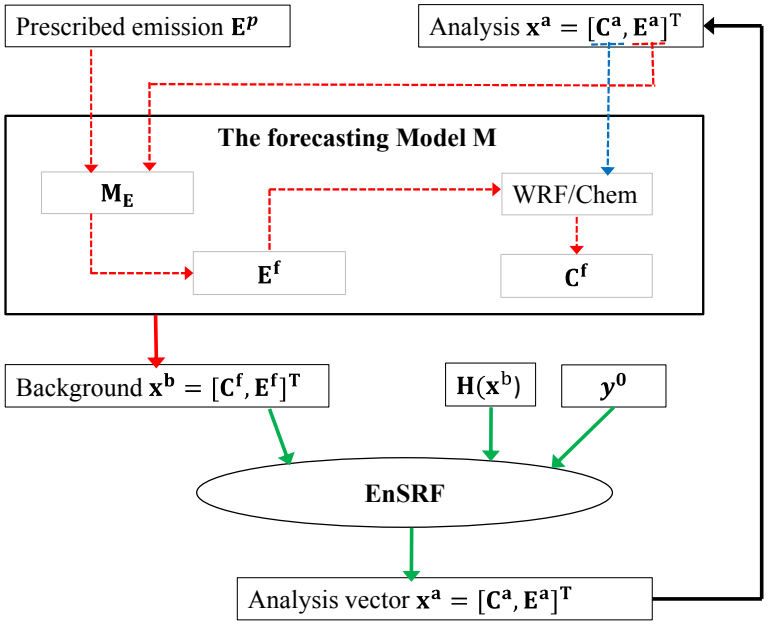

Figure 1. Flow chart of the data assimilation system that simultaneously optimizes the chemical initial conditions and emissions.

Atmos. Chem. Phys. Discuss., https://doi.org/10.5194/acp-2018-1152
Manuscript under review for journal Atmos. Chem. Phys.
Discussion started: 4 January 2019

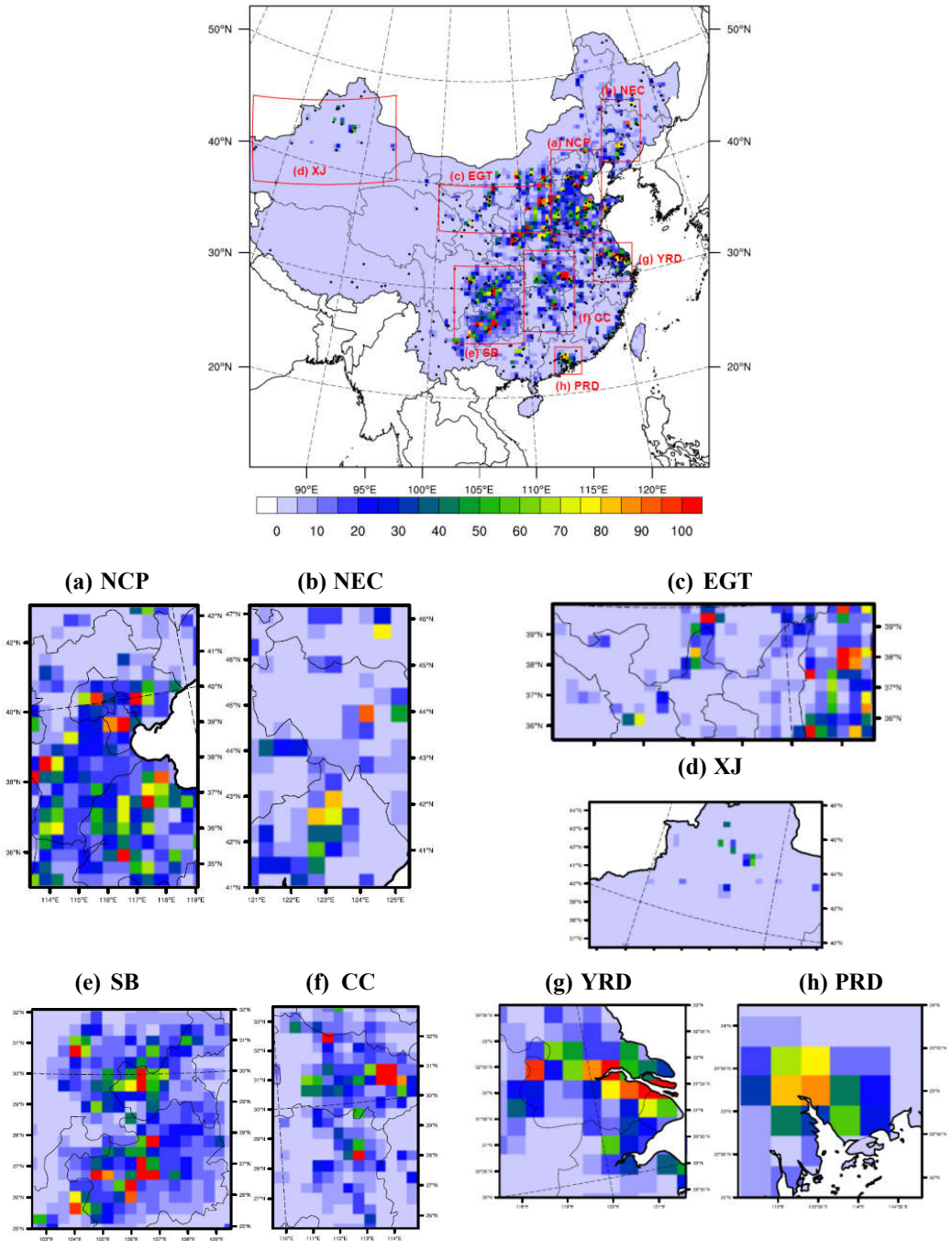

Figure 2. Spatial distribution of prior SO_2 emissions used in this study. Regions defined in red rectangles are: a-NCP (North China Plain), b-NEC (Northeastern China), c-EGT (Energy Golden Triangle), d-XJ (Xinjiang), e-SB (Sichuan Basin), f-CC (Central China), g-YRD (Yangzi River Delta), h-PRD (Pearl River Delta). Unit: mol km^{-2} h^{-1}.

Atmos. Chem. Phys. Discuss., https://doi.org/10.5194/acp-2018-1152
Manuscript under review for journal Atmos. Chem. Phys.
Discussion started: 4 January 2019

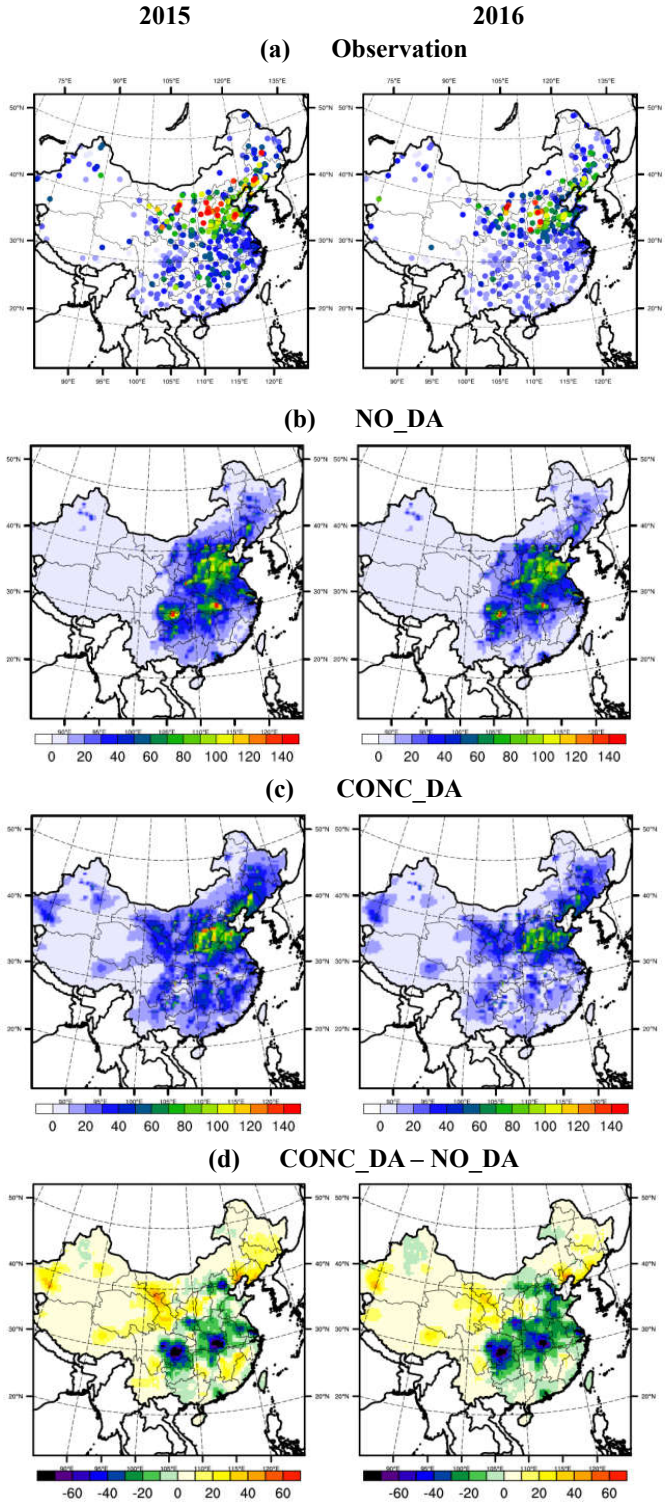

Figure 3. Observed and modeled monthly average of SO2 concentrations for January in 2015 (Left) and 2016 (right). (a) Observations, (b) NO_DA, (c) CONC_DA, (d) CONC_DA-NO_DA. Unit: μg m^{-3}.

Atmos. Chem. Phys. Discuss., https://doi.org/10.5194/acp-2018-1152
Manuscript under review for journal Atmos. Chem. Phys.
Discussion started: 4 January 2019

Atmospheric Chemistry and Physics Discussions

(a). 2015 - NO_DA (top) and CONC_DA (bottom)

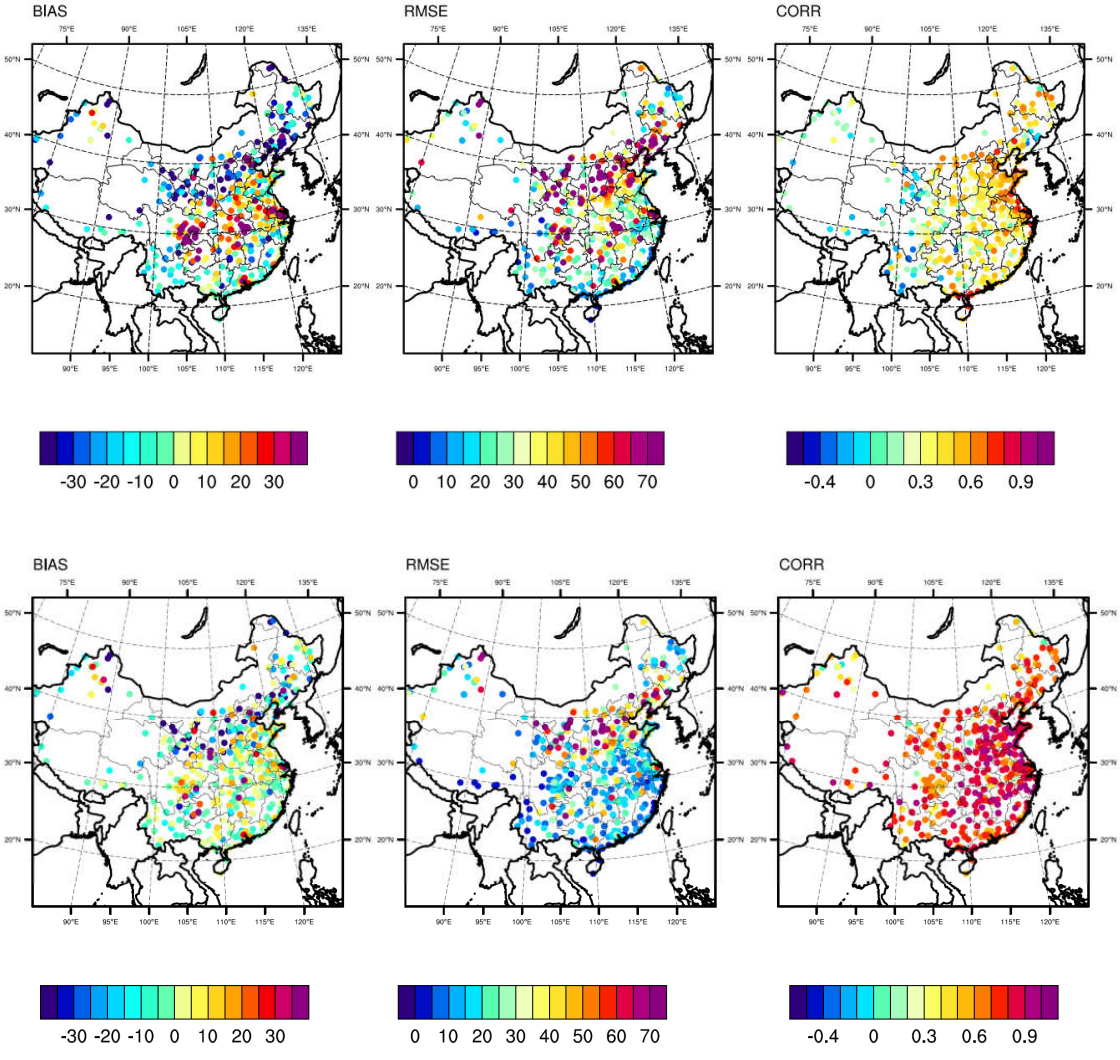

Figure 4. (a) The spatial distribution of statistics between model simulations and observations for January 2015. Top: NO_DA v.s. observation, bottom: CONC_DA v.s. observation. Units: μg m^{-3} for BIAS and RMSE.

Atmos. Chem. Phys. Discuss., https://doi.org/10.5194/acp-2018-1152
Manuscript under review for journal Atmos. Chem. Phys.
Discussion started: 4 January 2019

Atmospheric Chemistry and Physics Discussions

(b). 2016 - NO_DA (top) and CONC_DA (bottom)

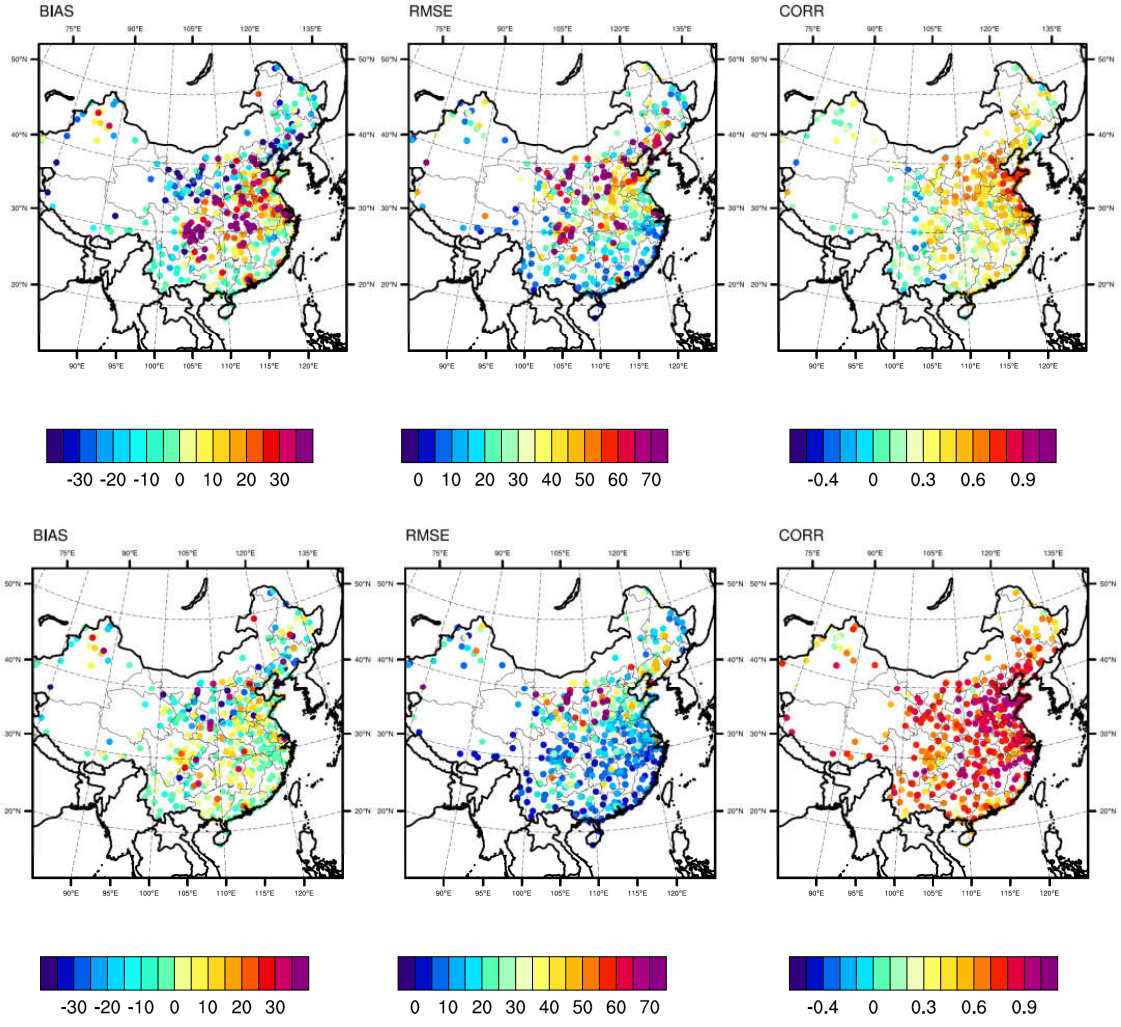

Figure 4. (b) Continue. Same as Figure 4a, but for 2016.

Atmos. Chem. Phys. Discuss., https://doi.org/10.5194/acp-2018-1152
Manuscript under review for journal Atmos. Chem. Phys.
Discussion started: 4 January 2019

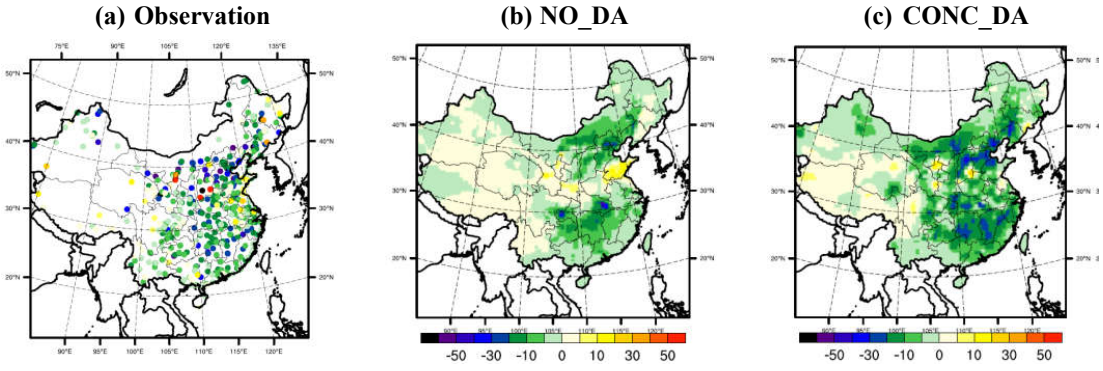

Figure 5. Observed and modeled SO_2 ambient concentration changes (January 2016 - January 2015). (a) Observations, (b) NO_DA, (c) CONC_DA. (Unit: μg m^{-3})

Atmos. Chem. Phys. Discuss., https://doi.org/10.5194/acp-2018-1152
Manuscript under review for journal Atmos. Chem. Phys.
Discussion started: 4 January 2019

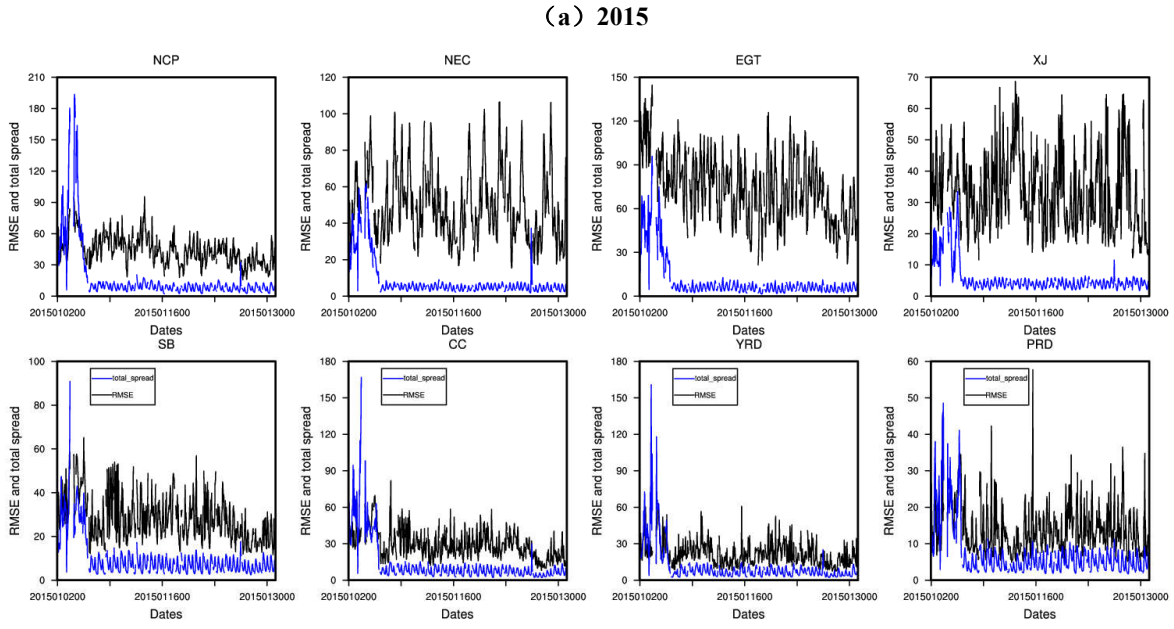

Figure 6. Regional averaged RMSE and total spread for (a) January 2015 and (b) January 2016 in 8 regions (Unit: μg m^{-3})

Atmos. Chem. Phys. Discuss., https://doi.org/10.5194/acp-2018-1152
Manuscript under review for journal Atmos. Chem. Phys.
Discussion started: 4 January 2019

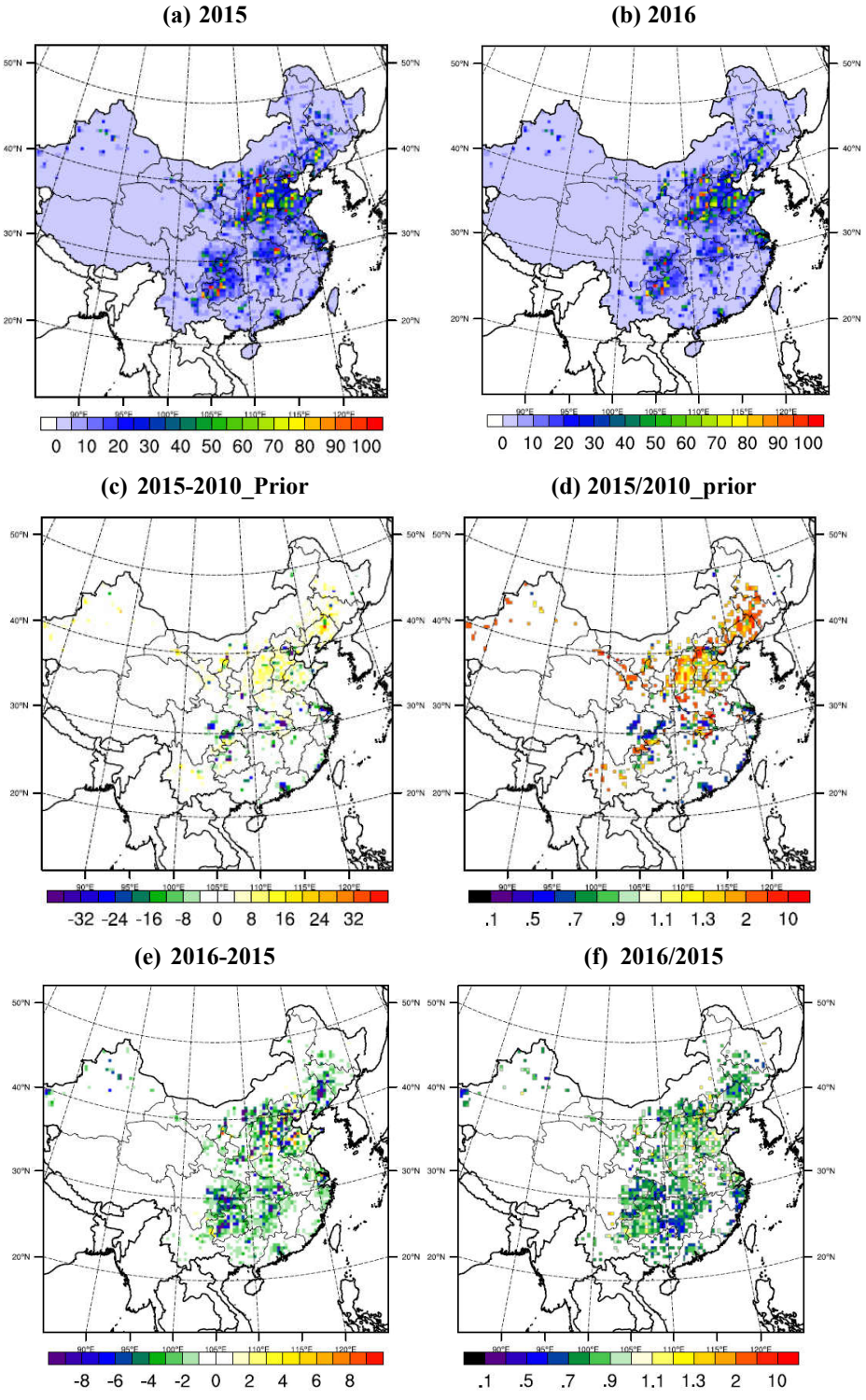

Figure 7. Analyzed emissions for (a) January 2015 and (b) January 2016. (c) The differences of 2015-2010_prior, (d) Ratios of 2015/2010_priori, (e) The differences of 2016-2015 and (f) Ratios of 2016/2015. Unit is mol km^{-2} h^{-1} for (a), (b), (c) and (e).

Atmos. Chem. Phys. Discuss., https://doi.org/10.5194/acp-2018-1152
Manuscript under review for journal Atmos. Chem. Phys.
Discussion started: 4 January 2019

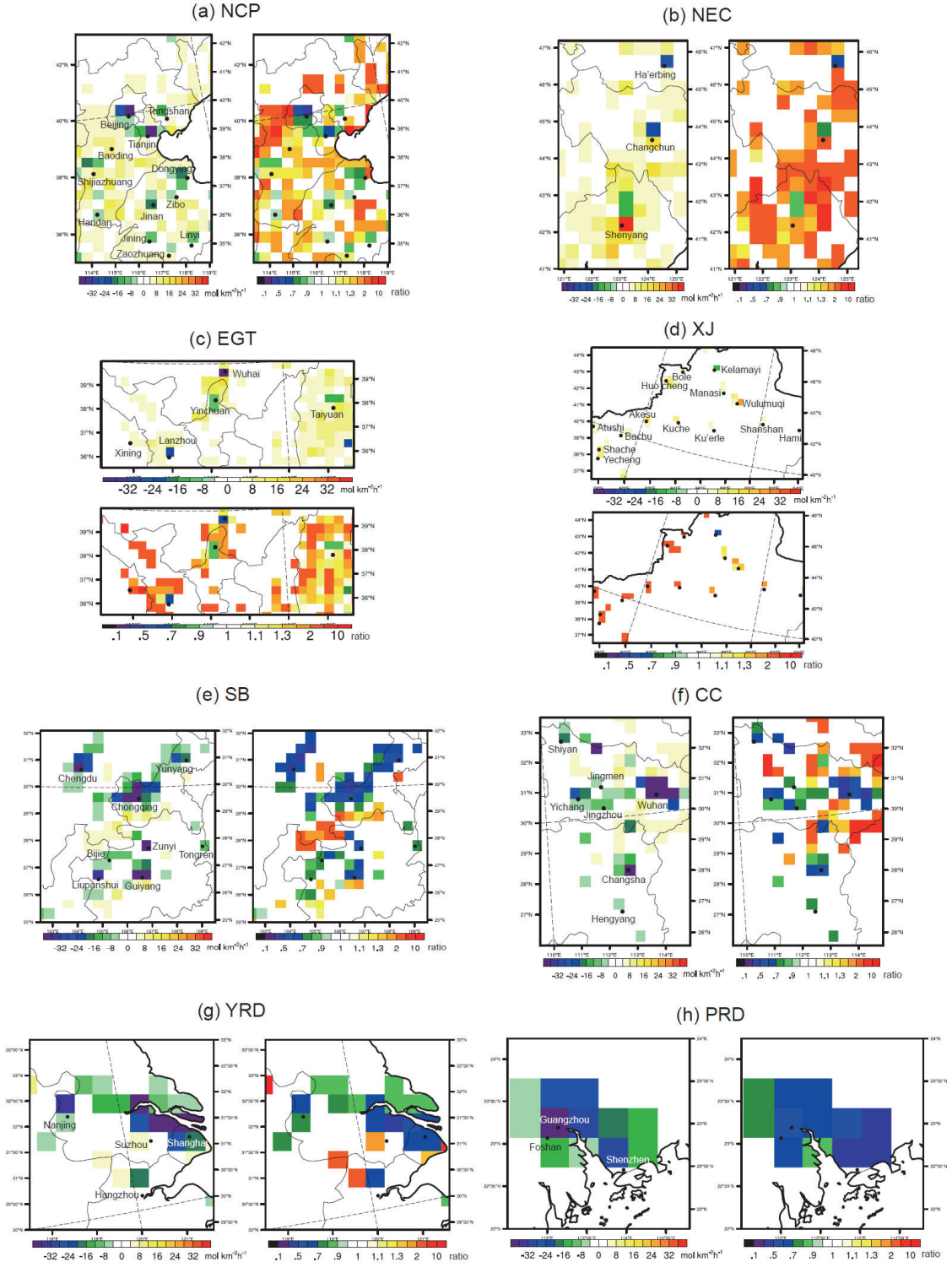

Figure 8. The differences of analyzed 2015 January emissions and 2010 priori emissions in 8 regions. Left panels are emission differences of 2015-2010 (unit: mol km^{-2} h^{-1}) and right panels are ratios of 2015/2010 in each region.

Atmos. Chem. Phys. Discuss., https://doi.org/10.5194/acp-2018-1152
Manuscript under review for journal Atmos. Chem. Phys.
Discussion started: 4 January 2019

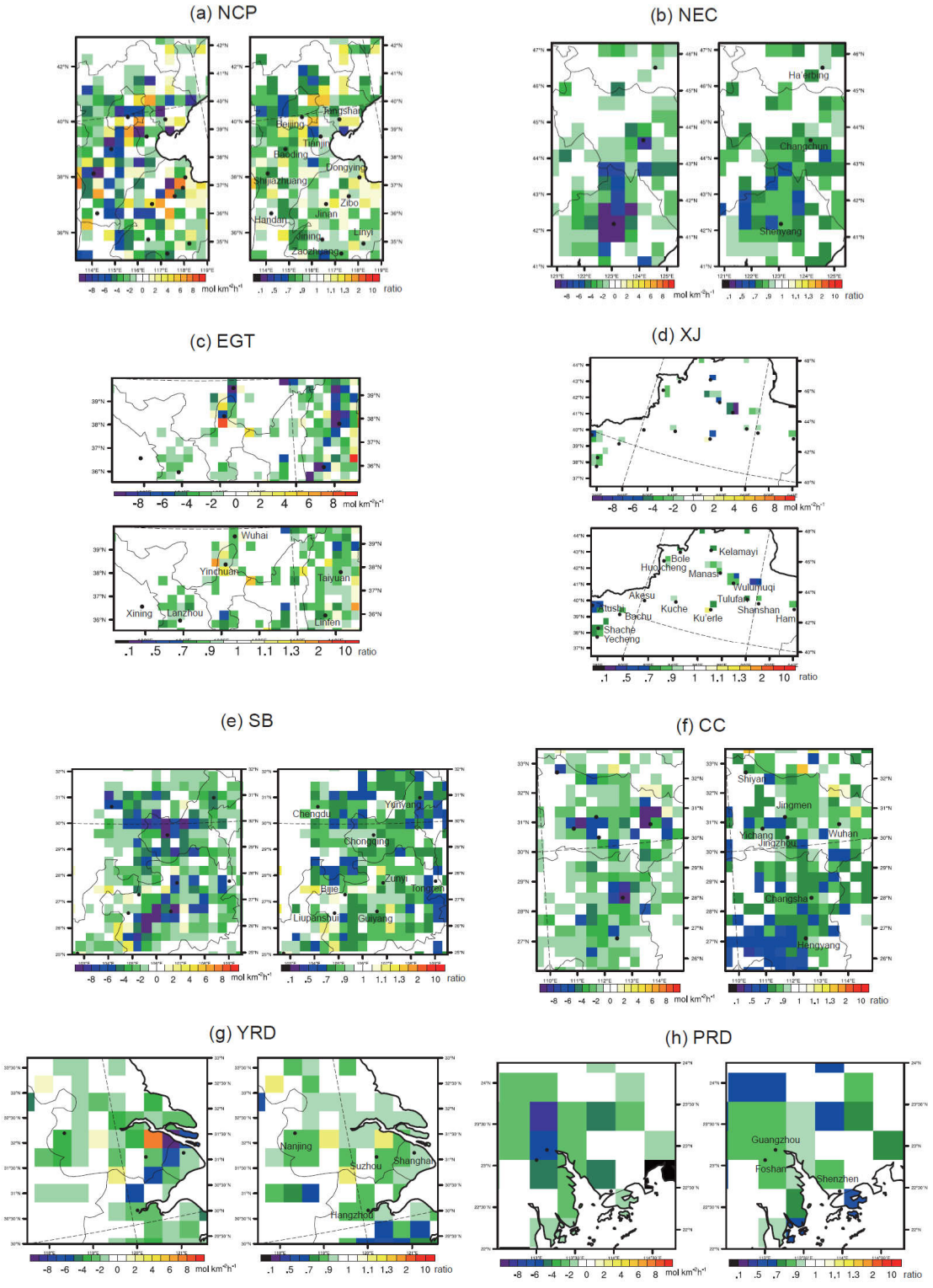

Figure 9. Same as Figure 8, but for the differences of analyzed 2016 January emissions and 2015 January emissions in 8 regions. Left panels are emission differences of 2016-2015 (unit: mol km^{-2} h^{-1}) and right panels are ratios 2016/2015 in each region.

Atmos. Chem. Phys. Discuss., https://doi.org/10.5194/acp-2018-1152
Manuscript under review for journal Atmos. Chem. Phys.
Discussion started: 4 January 2019

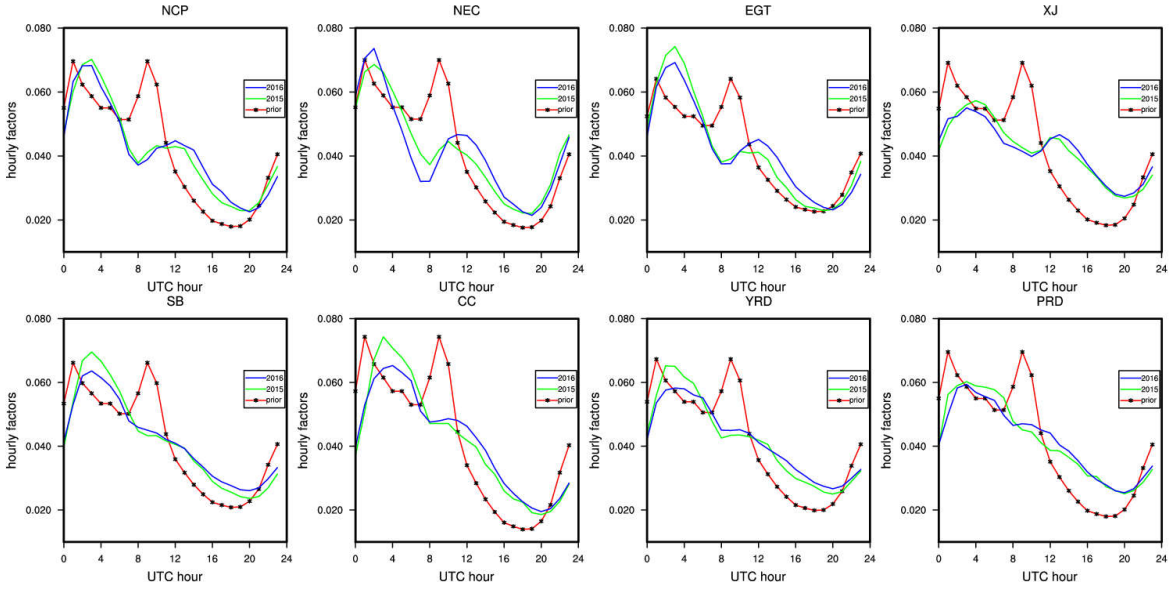

Figure 10. Hourly factors in priori emission inventory and derived from 2015January and 2016 January EMIS_DA experiment in 8 regions.

Atmos. Chem. Phys. Discuss., https://doi.org/10.5194/acp-2018-1152
Manuscript under review for journal Atmos. Chem. Phys.
Discussion started: 4 January 2019

Atmospheric Chemistry and Physics Discussions

(a) NO_DA_FCST

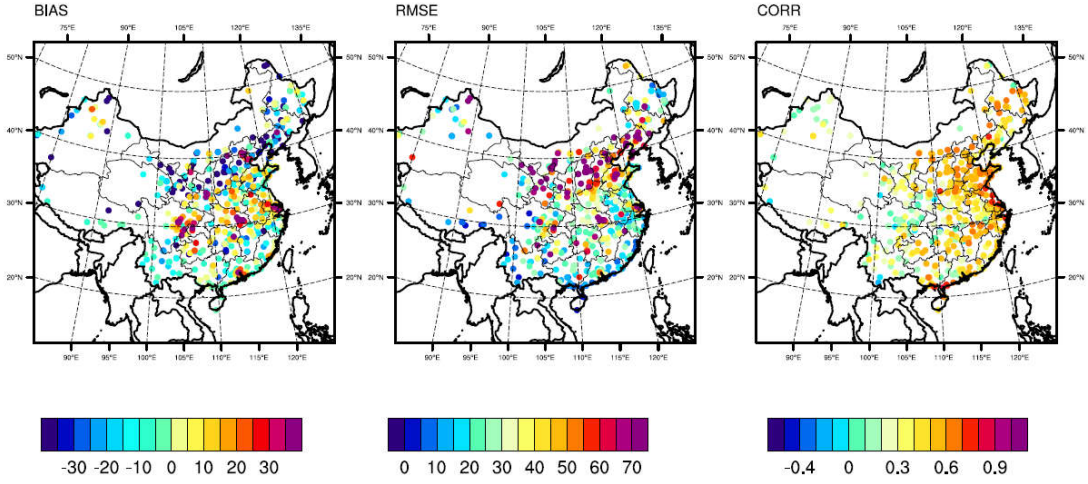

(b) Differences (EMIS_DA_FCST - NO_DA_FCST) - Group A

BIAS changes (%) **RMSE changes (%)** **CORR changes**

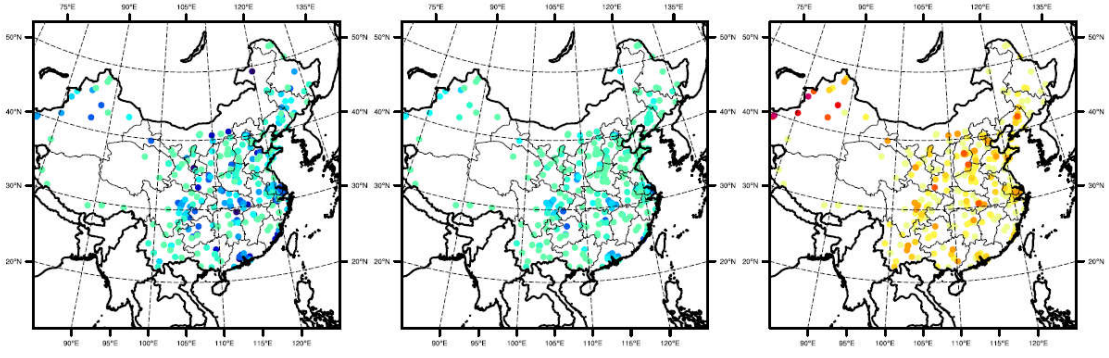

(c) Group B

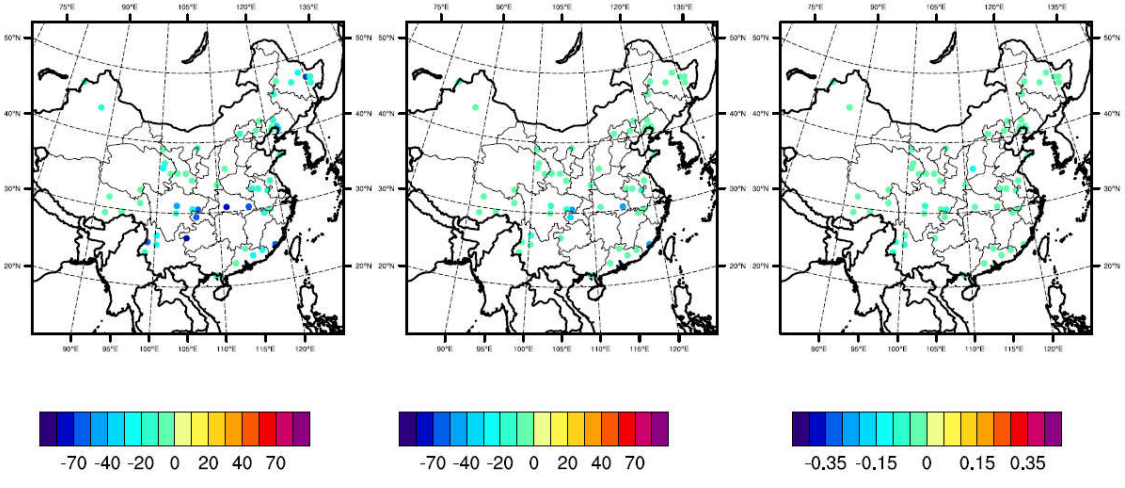

Atmos. Chem. Phys. Discuss., https://doi.org/10.5194/acp-2018-1152
Manuscript under review for journal Atmos. Chem. Phys.
Discussion started: 4 January 2019

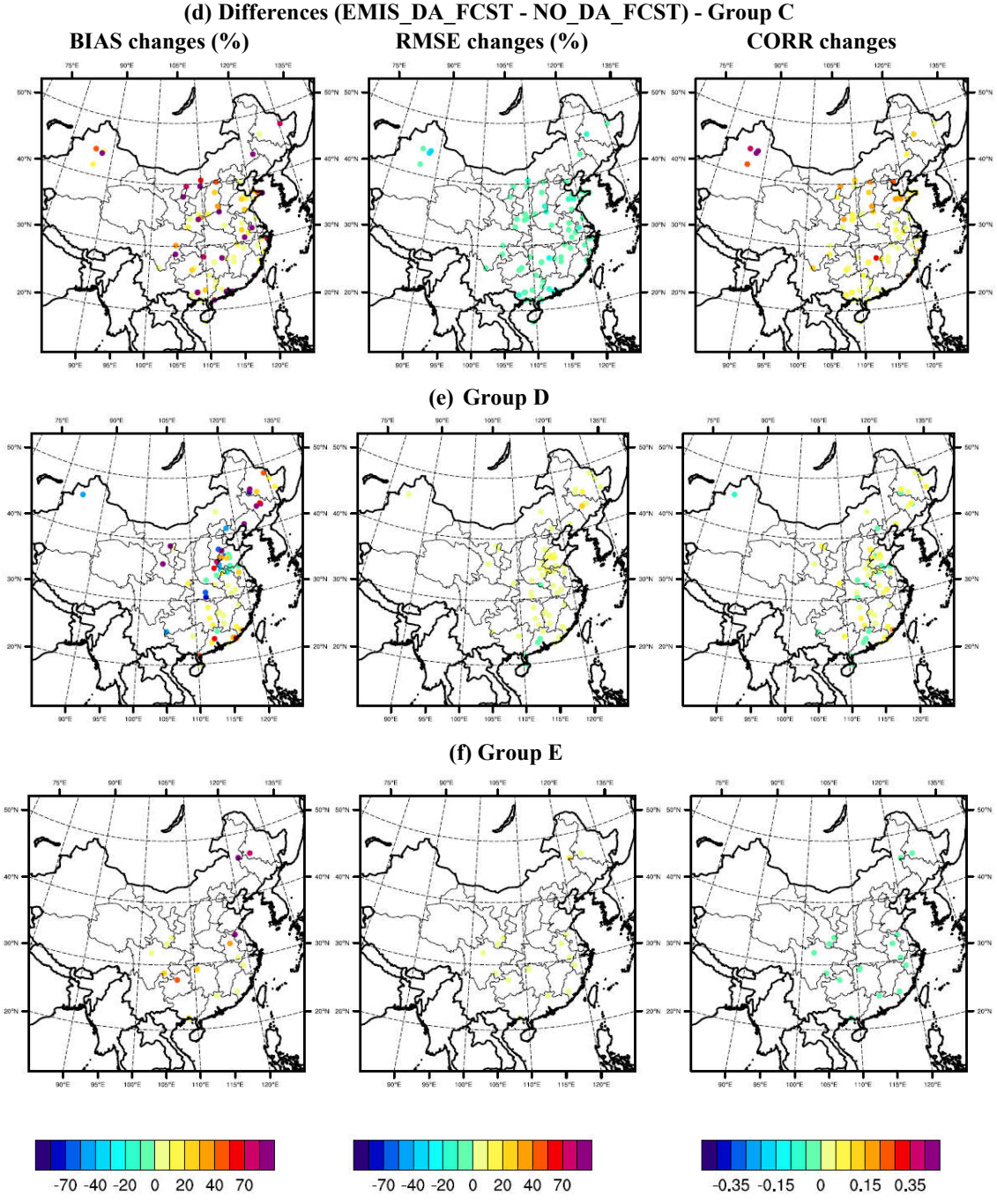

Figure 11. The spatial distribution of error statistics between model simulations and observations for January 2015. (a) Statistics between NO_DA_FCST and observations, BIAS and RMSE in μg m^{-3}; (b)-(f) are the statistics improvements from NO_DA_FCST to EMIS_DA_FCST for different groups of sites (classification in table 2), the BIAS and RMSE improvements are in percentage.

Atmos. Chem. Phys. Discuss., https://doi.org/10.5194/acp-2018-1152
Manuscript under review for journal Atmos. Chem. Phys.
Discussion started: 4 January 2019

Atmospheric Chemistry and Physics Discussions

(a) NO_DA_FCST

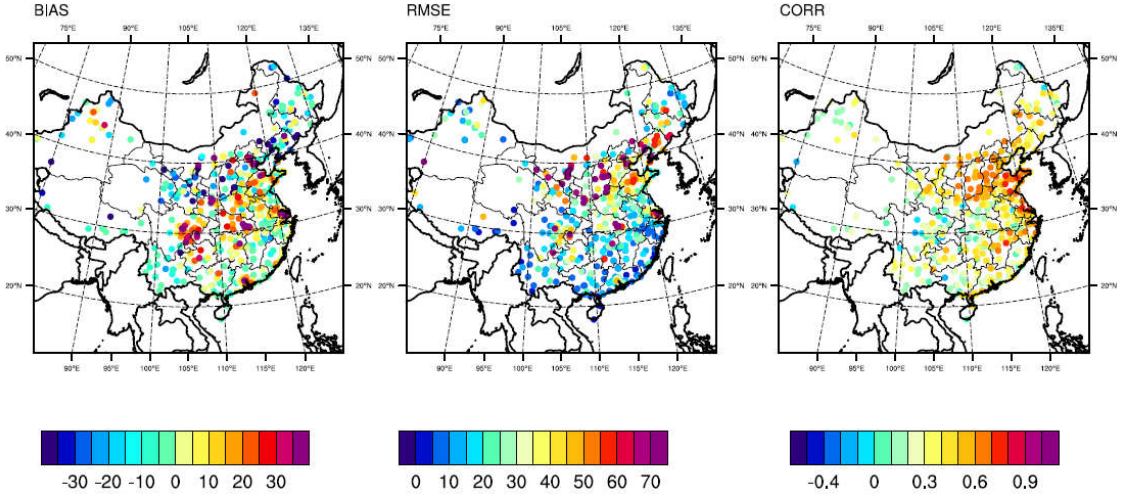

(b) Differences (EMIS_DA_FCST - NO_DA_FCST) - Group A

BIAS changes (%) **RMSE changes (%)** **CORR changes**

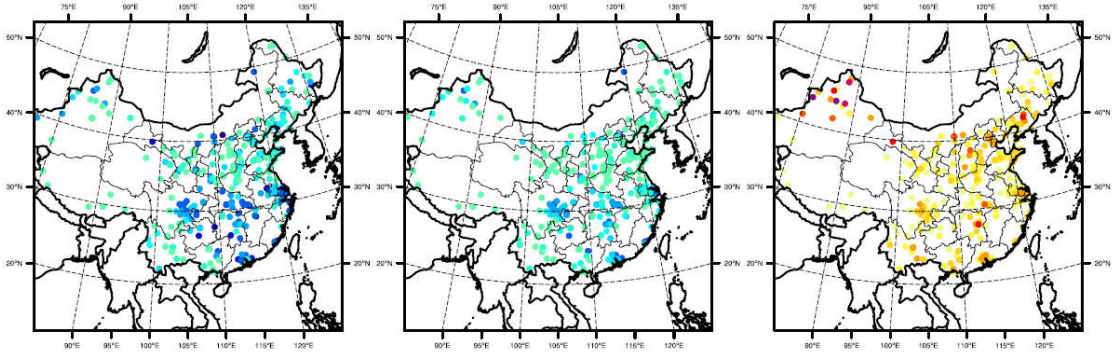

(c) Group B

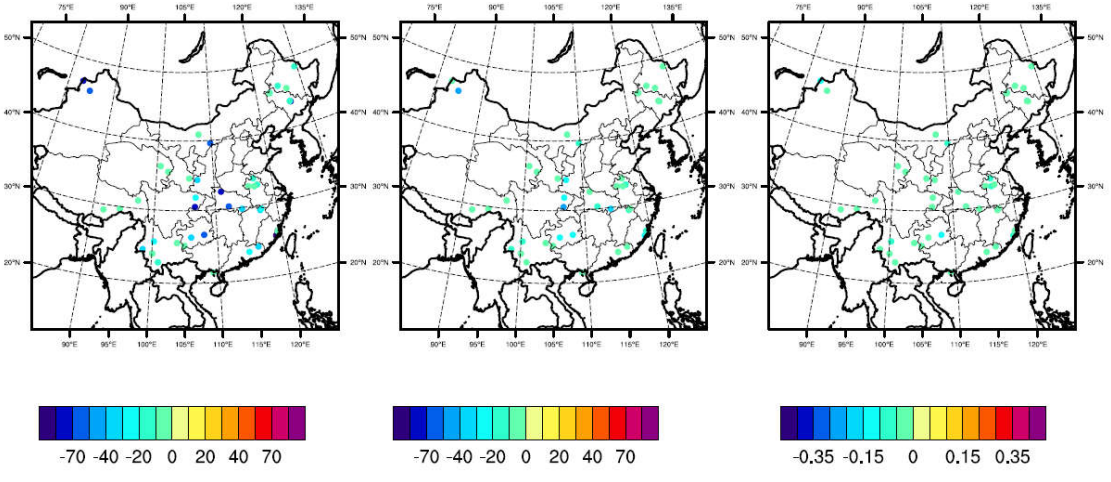

Atmos. Chem. Phys. Discuss., https://doi.org/10.5194/acp-2018-1152
Manuscript under review for journal Atmos. Chem. Phys.
Discussion started: 4 January 2019

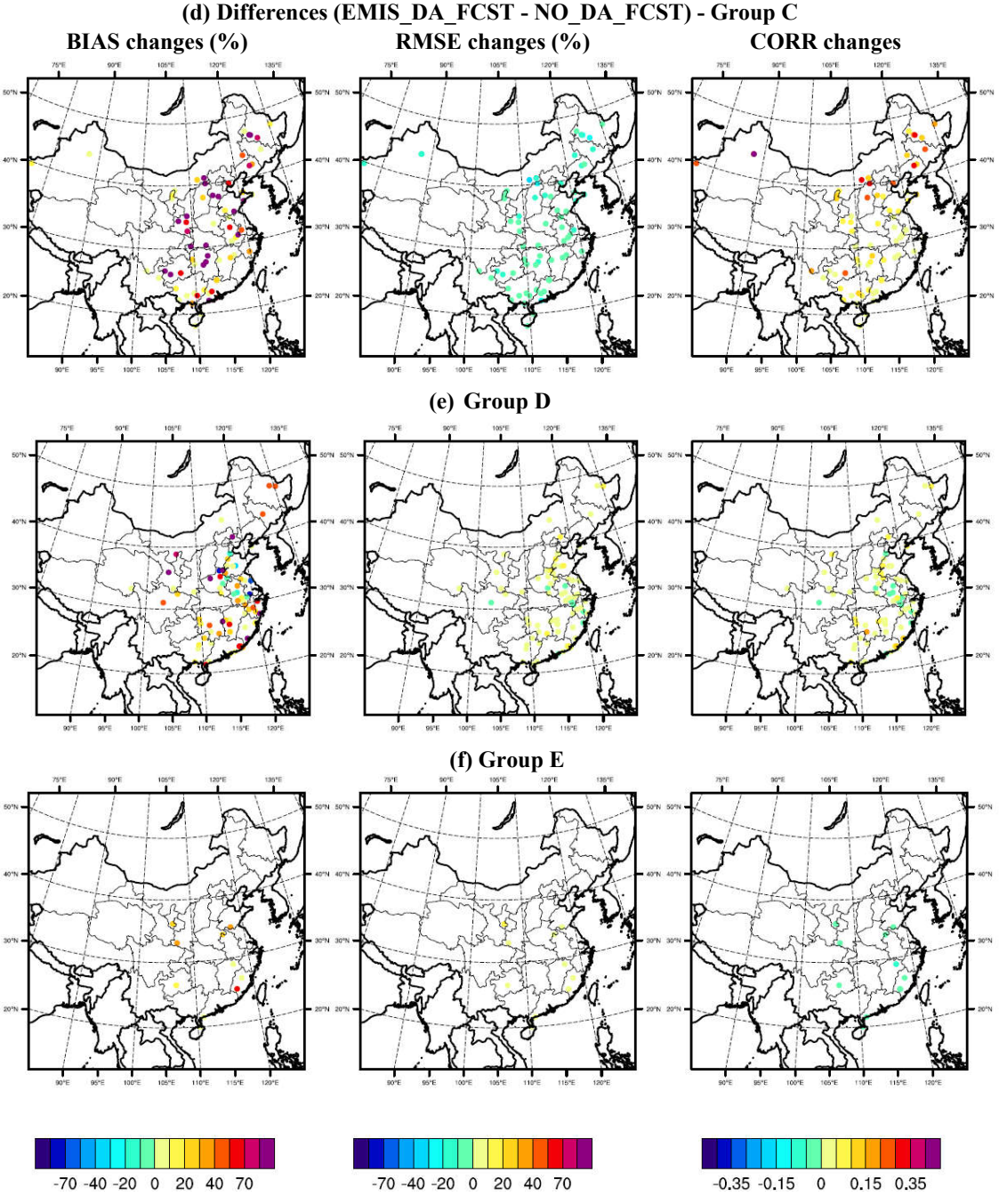

Figure 12. Same as Figure 11 but for January 2016.

Atmos. Chem. Phys. Discuss., https://doi.org/10.5194/acp-2018-1152
Manuscript under review for journal Atmos. Chem. Phys.
Discussion started: 4 January 2019

Atmospheric Chemistry and Physics Discussions

(a)

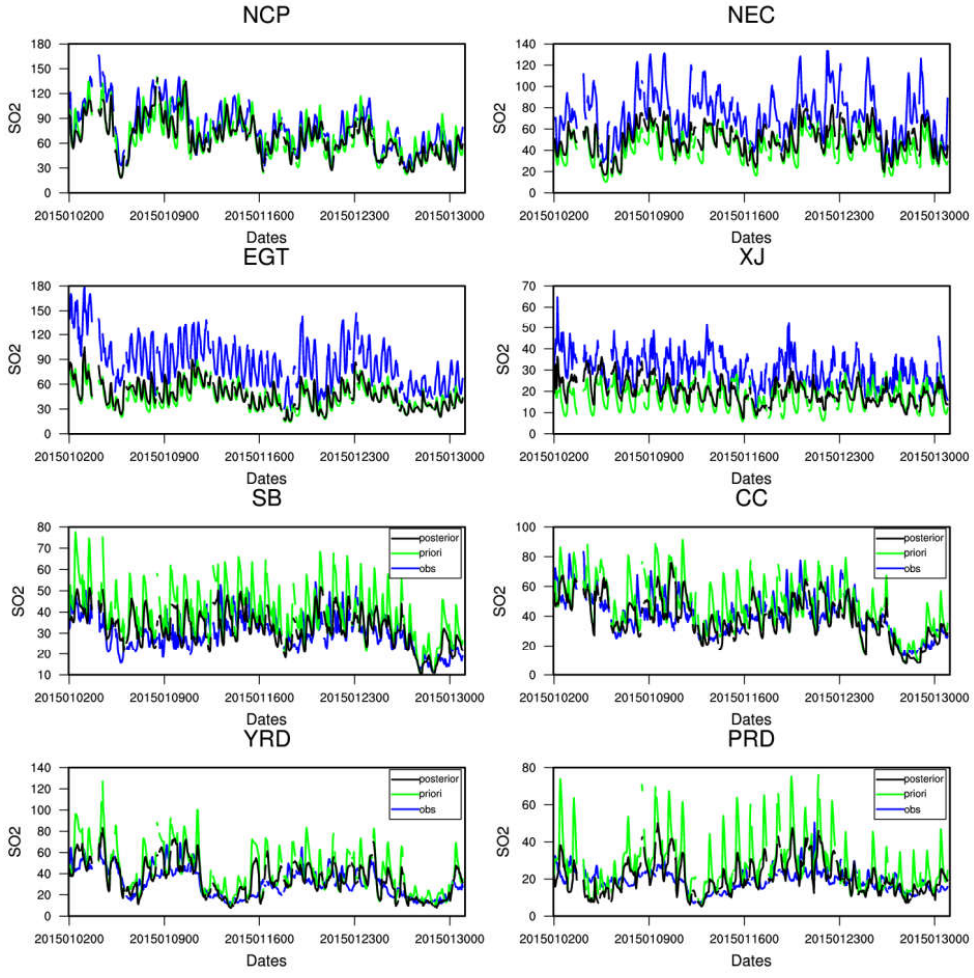

Figure 13. Time series of regional mean SO_2 concentrations from observations and model simulations with priori and analyzed (posterior) emissions for (a) January 2015 and (b) January 2016 in 8 regions. (Unit: μg m^{-3})

Atmos. Chem. Phys. Discuss., https://doi.org/10.5194/acp-2018-1152
Manuscript under review for journal Atmos. Chem. Phys.
Discussion started: 4 January 2019

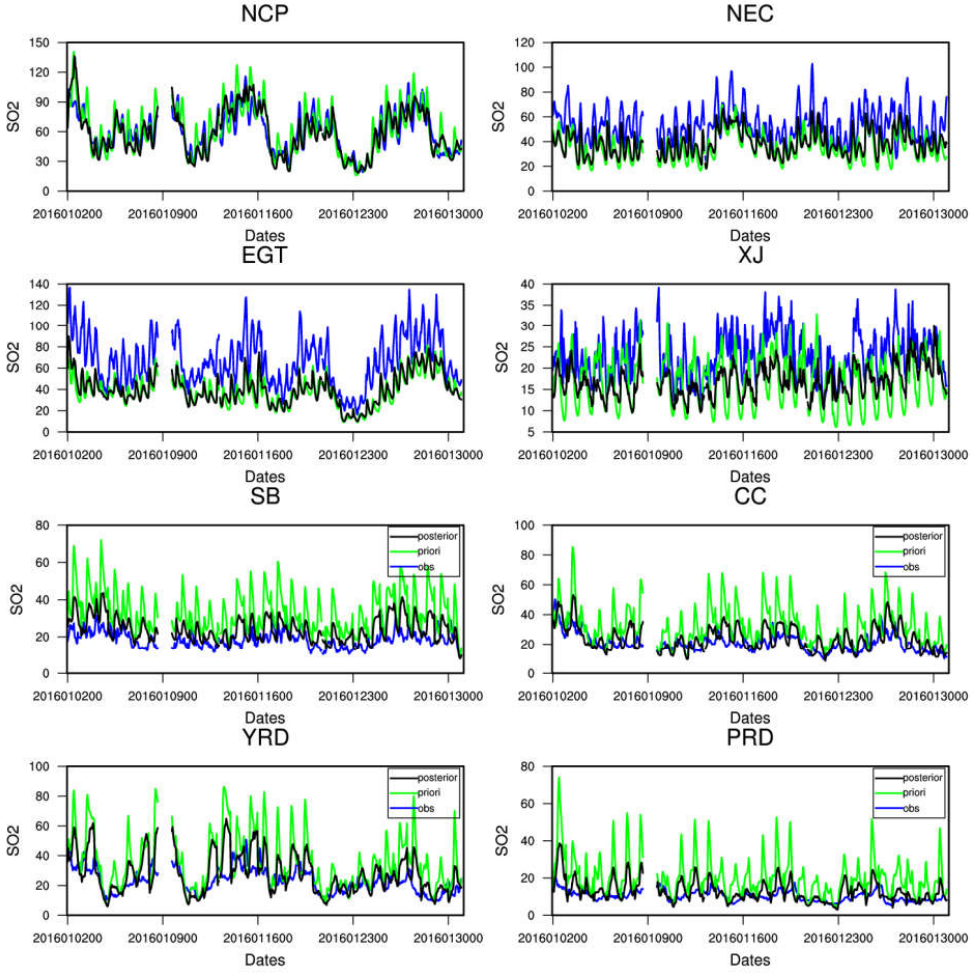

Figure 13(b)